An RNA-based feed-forward mechanism ensures motor switching in *oskar* mRNA transport

Imre Gáspár[1,2] *, Ly Jane Phea[1], Mark A. McClintock[3], Simone Heber[1], Simon L. Bullock[3] * and Anne Ephrussi[1] *

1 Developmental Biology Unit, European Molecular Biology Laboratory, 69117 Heidelberg, Germany

2 Current address: Max Planck Institute of Biochemistry, Martinsried, Germany.

3 Division of Cell Biology, MRC Laboratory of Molecular Biology, Cambridge, United Kingdom

*Correspondence: gaspar@biochem.mpg.de, sbullock@mrc-lmb.cam.ac.uk, anne.ephrussi@embl.org

Abstract

Regulated recruitment and activity of motor proteins is essential for intracellular transport of cargoes, including ribonucleoprotein complexes (RNP). Here we show that orchestration of *oskar* RNP transport in the *Drosophila* germline relies on the interplay of two double-stranded RNA binding proteins, Staufen and the dynein adaptor Egalitarian (Egl). Following delivery of nurse cell-synthesized *oskar* mRNA into the oocyte by dynein, enhanced recruitment of Staufen to the RNPs results in dissociation of Egl and reduced minus end-directed transport without overtly affecting overall dynein levels on the cargo. This mechanism allows kinesin-1 to translocate the mRNA to its final destination at the posterior pole of the oocyte. Using *in vitro* motility assays with purified components, we find that Staufen directly antagonizes Egl-mediated activation of *oskar* mRNA transport by dynein. We additionally show that Egl associates with *staufen* mRNA in the nurse cells and mediates enrichment of the mRNA and its protein product in the ooplasm. Our observations identify a feed-forward mechanism, whereby dynein-dependent accumulation of *staufen* mRNA and protein in the oocyte enables motor switching during *oskar* mRNA transport by downregulating dynein activity.

Introduction

Proper execution of the genetic program relies on regulatory mechanisms that act at multiple levels of gene expression, from transcription to post-translational events, such as protein modification or RNA decay. In large cells, such as neurons, early embryos and oocytes, a key process that regulates genetic output at the subcellular level is RNA localization, which is often driven by cytoskeletal motors (Gaspar 2011; Glock et al. 2017; Marchand et al. 2012; St Johnston 2005; Mofatteh and Bullock 2017 Eliscovich and Singer, 2017). The kinesin-1 and cytoplasmic dynein-1 (dynein) motors, which move mRNPs towards the plus end and minus end of microtubules, respectively, have been implicated in mRNA trafficking in several systems (Gaspar, 2011; Mofatteh and Bullock, 2017).

A paradigm for the study of microtubule-based mRNP transport is *oskar* mRNA, which is produced in the nurse cells of the *Drosophila* germline syncytium in the early stages of oogenesis and transported by dynein into the developing oocyte where microtubule minus ends are enriched (Clark et al., 2007; Ephrussi et al., 1991; Kim-Ha et al, 1991; Jambor et al., 2014; Januschke et al., 2002; Sanghavi et al., 2013; Vazquez-Pianzola et al., 2017). Trafficking of mRNAs from the nurse cells to the oocyte is dependent on the Egalitarian (Egl) protein, which binds specialized stem-loop structures in localizing mRNAs and links them together with its coiled-coil binding partner Bicaudal-D (BicD) to dynein and the dynein activating complex dynactin (Navarro et al. 2004; Dix et al. 2013; Dienstbier et al. 2009). During mid-oogenesis, when the microtubule cytoskeleton is reorganized, many Egl target mRNAs become localized at the anterior of the oocyte, where microtubule minus ends are now concentrated (Gaspar 2011; Lasko 2012). In contrast, *oskar* mRNA is transported at this stage to the posterior pole by the Kinesin-1 heavy chain (Khc) (Brendza et al., 2000; Palacios and St Johnston, 2002; Williams et al., 2014; Zimyanin et al., 2008), where the microtubule plus ends are focused (Parton et al., 2011; Sanghavi et al., 2013). Khc is already recruited to

oskar mRNPs in the nurse cells (Gáspár et al., 2017) raising the question of how the activity of the motor is coordinated with that of dynein during delivery of *oskar* mRNA from the nurse cells to the oocyte posterior.

Another double-stranded RNA binding protein (dsRBP), Staufen, is necessary for the Khc-mediated localization of *oskar* to the posterior pole (Ephrussi et al., 1991; Kim-Ha et al, 1991; St Johnston et al., 1992; Zimyanin et al., 2008). Staufen is also required for production of Oskar protein, which induces abdomen and germline formation in the embryo (Ephrussi and Lehmann, 1992; Markussen et al., 1995; Micklem et al., 2000). Staufen is also involved in trafficking of other mRNAs, such as *bicoid* in the oocyte and *prospero* in dividing neuroblasts (Ferrandon et al., 1994; Schuldt et al., 1998). Mammalian orthologues of *Drosophila* Staufen, mStau1 and mStau2, play roles in the bidirectional transport of *CaMKIIα* and *Rgs4* mRNAs in dendrites (Bauer et al., 2019; Heraud-Farlow et al., 2013) and in Xenopus oocytes, Staufen is a component of *Vg1* transport RNPs (Yoon and Mowry 2004), indicating that Staufen's function as a regulator of RNP transport is evolutionarily conserved. Supporting this notion, mStau2 can partially substitute for *Drosophila* Staufen in *oskar* mRNA localization (Heber et al., 2019). How Staufen proteins orchestrate mRNA trafficking processes is unclear.

Here, we show that Staufen antagonizes minus-end-directed transport of *oskar* mRNA by dynein within the *Drosophila* oocyte. Recombinant Staufen can also inhibit transport of *oskar* mRNA *in vitro* by purified Egl, BicD, dynein and dynactin, showing that it is a direct regulator of the transport machinery. Staufen inhibits dynein-based transport of *oskar* mRNA by displacing Egl from the RNPs once they have reached the oocyte and thus allows kinesin-1 to translocate the mRNA to the posterior pole of this cell. We provide evidence that Staufen's inhibition of dynein is restricted to the oocyte by Egl- and dynein-mediated concentration of nurse cell-synthesized *staufen* mRNA in the ooplasm. Thus, Egl delivers its own negative regulator into the oocyte, constituting a feed-forward regulatory mechanism that spatially and temporally controls dynein activity and thus *oskar* mRNA localization during oogenesis.

Results

Staufen suppresses minus end-directed transport of *oskar* mRNPs in ooplasmic extracts

oskar mRNA is localized at the posterior pole of the oocyte during mid-oogenesis (Fig 1A and Ephrussi et al. 1991; Kim-Ha et al. 1991). In *staufen* mutant oocytes, enrichment of *oskar* mRNA at the posterior pole is greatly reduced, and a considerable amount of *oskar* remains at the anterior margin of the oocyte (Fig 1A'; Ephrussi et al., 1991). High-resolution analysis of the movement of GFP-labelled *oskar-MS2* mRNPs in *stau* RNAi ooplasmic extracts by TIRF microscopy (Video S3 and S4; Gaspar and Ephrussi, 2017; Gáspár et al., 2017) revealed that the ~ 2:1 dominance of microtubule plus end- versus minus end-directed *oskar* mRNP runs observed in wild-type samples is lost, and there is no overt bias in the directionality of motility (Fig 1B). The distribution of *oskar* mRNA and the directionality of mRNP transport in *staufen* mutants differ from what is observed in other mutants affecting

oskar localization: in *Tm1*^{gs} (Fig 1A" and (Gáspár et al., 2017) and *Khc*^{null} (Brendza et al., 2000; Gáspár et al., 2017; Williams et al., 2014; Zimyanin et al., 2008) mutants, *oskar* mRNA fails to localize at the posterior of the oocyte, and minus-end-directed transport predominates (Gáspár et al., 2017).

To investigate the basis of the posterior localization defect in *staufen* mutants, we quantified the colocalization of functional, endogenously tagged fluorescent Khc molecules and *oskar* mRNA detected by smFISH. This method was previously used to show that Tm1 mutations reduce the association of *oskar* mRNPs with the motor (Gáspár et al., 2017). In the absence of Staufen, there was no reduction in Khc association with the mRNPs in either the nurse cells or the oocyte (Fig 1C). Moreover, analysis of the speed and length of *oskar* RNP runs in ooplasmic extracts indicated that Khc activity was not compromised upon *staufen* knock-down (Fig 1D and E). Interestingly, however, runs towards microtubule minus ends were faster and longer compared to the wild type (Fig 1D and E), indicating that the loss of plus end dominance of *oskar* mRNP runs is associated with hyperactivity of the minus end-directed dynein transport machinery. Previous work with gain-of-function mutations in the dynein adaptor BicD showed that increased dynein activity leads to ectopic anterior accumulation of *oskar* RNA (Liu et al., 2013; Navarro et al., 2004), as is observed in *staufen* mutant oocytes (Fig 1A', Ephrussi et al. 1991). Altogether, these findings point to a role of Staufen in suppression of minus end-directed transport of *oskar* RNA by dynein.

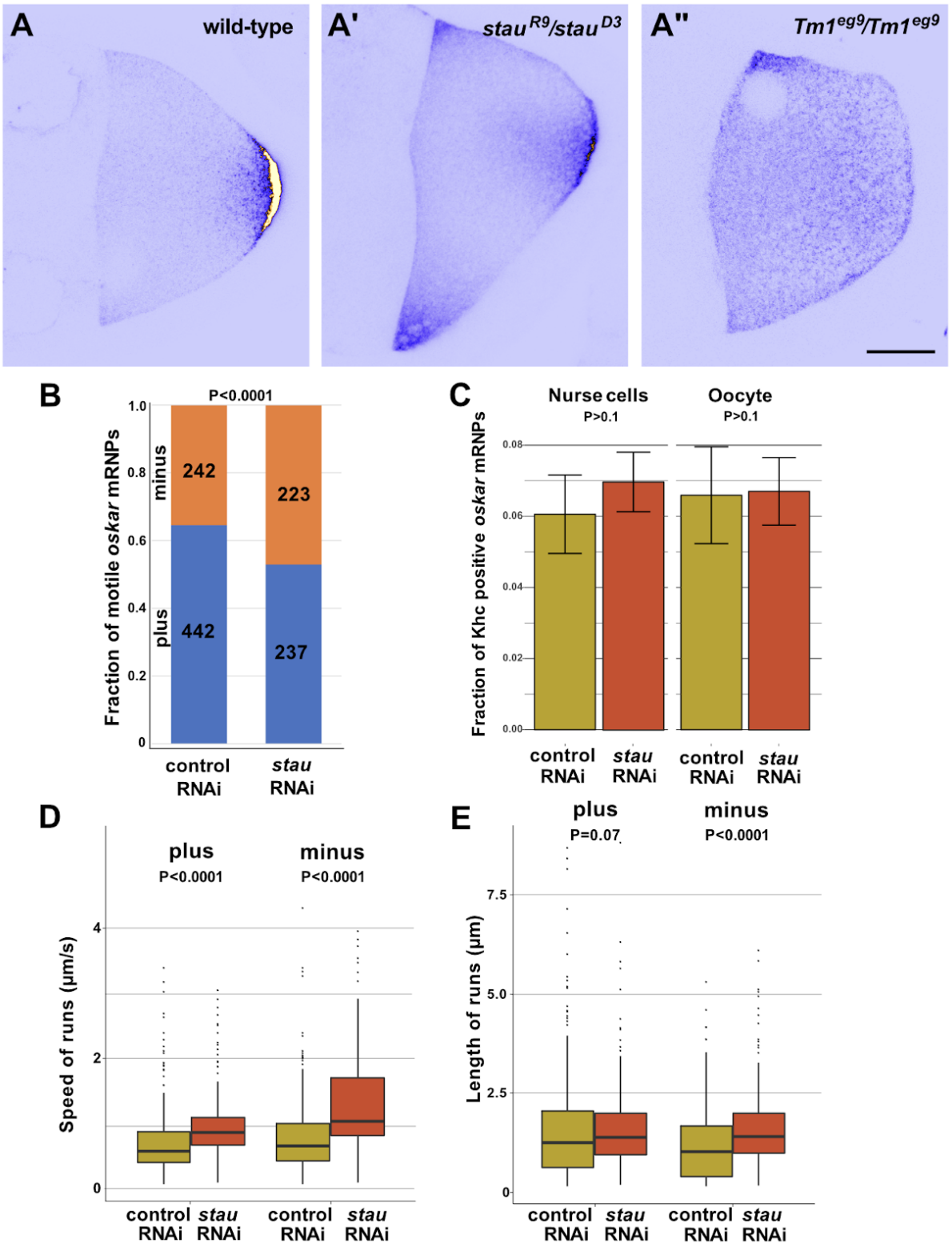

Figure 1: Effects of loss of Staufen on *oskar* RNA localization and transport. (A-A") Localization of *oskar* mRNA in wild-type (A), Staufen null (A') and Tm1-I/C null oocytes (A"). Scale bar represents 20 µm. (B) Polarity distribution of *oskar* mRNP runs *ex vivo* in the presence (control RNAi) or absence of Staufen (*stau* RNAi). Numbers indicate the number of *oskar* mRNP runs measured in the corresponding category. See also Video S3 and S4. (C) Khc association with *oskar* mRNPs *in situ* in the nurse cells and in the oocyte, in presence (brown) or absence (red) of Staufen. P-values of pairwise Student's t-tests are shown. (D-E) Speed

(D) and travelled distance (E) of motile *oskar* mRNPs *in vivo*, towards the plus or minus ends of microtubules in the presence (brown) and absence (red) of Staufen. P-values of Fisher exact (B) or pairwise Mann Whitney U-tests (C-E) are shown.

Staufen antagonizes dynein-mediated *oskar* mRNA transport by purified components

To test if Staufen has a direct inhibitory effect on minus-end directed *oskar* mRNP transport, we made use of an *in vitro* motility assay based on the reconstitution of a minimal RNP assembled from purified Egl, BicD, dynactin, fluorescently labelled dynein and *in vitro* transcribed RNA (McClintock et al. 2018). Motility of this RNP along immobilized, fluorescent microtubules can be visualized by TIRF microscopy using dyes on the mRNA and dynein.

In these experiments we used a ~529 nt fragment of the *oskar* 3'UTR that is sufficient for nurse cell to oocyte transport (Jambor et al. 2014). In the presence of Egl, BicD and dynactin, *oskar* mRNA frequently underwent long-distance transport in association with dynein (Fig. 2A and Fig S2A). No transport of *oskar* was observed when Egl and BicD were omitted from the mix (Fig. S2A); in this condition, we almost never observed association of *oskar* with microtubules or processive movement of microtubule-bound dynein complexes (Fig. S2A-C). These observations corroborate the conclusion that Egl and BicD link mRNAs to dynein-dynactin and activate movement of the motor along microtubules (Dienstbier et al. 2009; McClintock et al. 2018; Sladweski et al. 2018).

Addition of recombinant Staufen to the Egl, BicD, dynein and dynactin assembly mix significantly reduced the number of *oskar* mRNA transport events (Fig. 2A and B). This effect was associated with fewer mRNAs being recruited to the microtubule (Fig. 2C). However, those mRNAs that interacted with the microtubule were just as likely to undergo long-distance transport as those incubated without Staufen (Fig. 2D). These data show that Staufen directly inhibits transport of *oskar* by Egl, BicD, dynactin and dynein.

The number of dynein transport events was also lowered by Staufen (Fig. 2E). The number of microtubule-binding events of the motor was not, however, significantly reduced (Fig. 2F). Together with the reduced association of *oskar* mRNA with the microtubule (Fig. 2C), this result suggests that Staufen interferes with association of the RNA with the motor. Staufen did significantly reduce the proportion of microtubule-associated dyneins that underwent processive movement (Fig. 2G), which explains the decrease in the number of transported motor complexes. This behavior is expected when recruitment of RNA to dynein is impaired, as the ability of Egl and BicD to activate movement of the motor is strongly stimulated by binding of RNA to Egl (McClintock et al. 2018; Sladewski et al. 2018). Together, these observations indicate that Staufen interferes with Egl-mediated activation of dynein on *oskar* mRNPs.

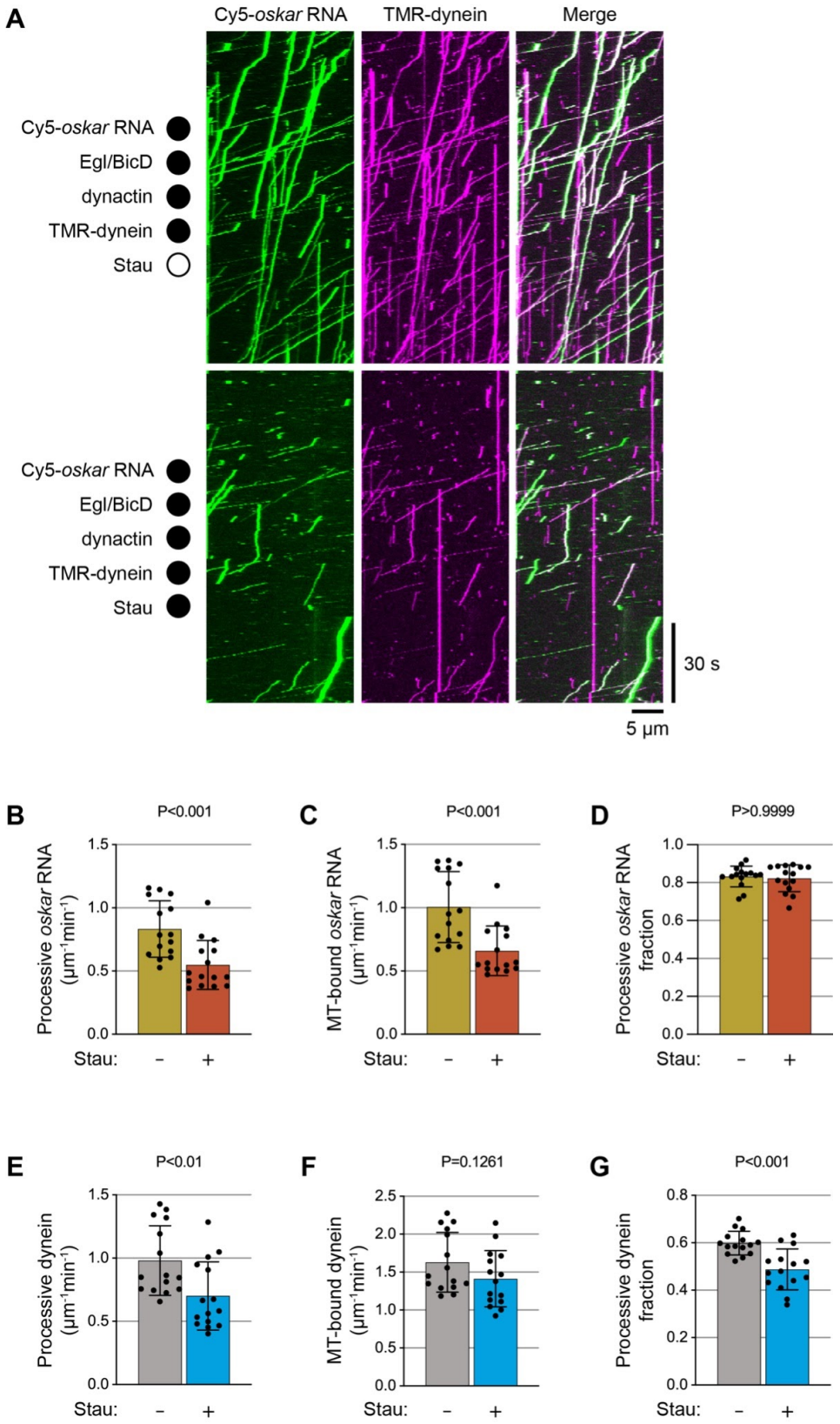

Figure 2. Staufen impedes *oskar* mRNA transport and dynein activation *in vitro*. (A) Example kymographs (time-distance plots) showing the behavior of *oskar* RNA and dynein in the presence and absence of Staufen; in both conditions, Egl, BicD and dynactin are also present but not fluorescently labelled (filled and empty circles represent the presence and absence of indicated proteins, respectively). Egl and BicD were coexpressed and copurified (see Methods). (B-G) Quantification of motile properties of *oskar* RNA (B-D) and dynein (E-G) in the conditions shown

in A. Charts show number of processive complexes (B, E), total number of microtubule (MT) binding events (C, F) and fraction of microtubule-binding events that result in processive motility (D, G). Mean ± SD of values from individual microtubules (represented by black circles) are displayed. Statistical significance and P-values were determined with Mann-Whitney tests.

A balance of Staufen and Egl is required for *oskar* mRNA localization *in vivo*

We next explored the interplay between Egl and Staufen function *in vivo* by manipulating the dosage of these proteins and determining the effects on *oskar* mRNA localization in mid-oogenesis. To obtain a representative, quantitative view of *oskar* mRNA distribution in oocytes, we applied an established statistical averaging method (Ghosh et al. 2012; Gaspar et al. 2014). In agreement with previous reports (Ephrussi et al., 1991; Kim-Ha et al. 1991), we found ectopic anterior accumulation of *oskar* in stage 9 oocytes of Staufen mutants, as indicated by the strong signal for the RNA in the anterior "corners" of the oocyte cortex, and a weak enrichment of *oskar* at the posterior (Fig 3A,B and Fig S1 A, B, E). A similar phenotype was observed upon UAS/Gal4-mediated overexpression of Egl in the germline (Fig 3C).

These observations suggest that Staufen and Egl antagonize one another in the context of *oskar* mRNA localization. To test this hypothesis, we overexpressed both GFP-Staufen and Egl in the germline and examined *oskar* localization at mid-oogenesis. While GFP-Staufen overexpression has no major effect on the localization of *oskar* (Fig S1F-I and Heber et al, 2019), it suppressed the ectopic anterior localization of *oskar* mRNA caused by elevated Egl levels (Fig 3C, D), consistent with a mutual antagonism of the dsRBPs. Further supporting this notion, removal of a functional copy of *egl* in egg-chambers with reduced Staufen levels (*stau* RNAi, egl^{1}/+), partially suppressed *oskar* mislocalization (Fig S3C-E). Overexpression of Staufen also suppressed the ectopic anterior localization of *oskar* mRNA caused by two different dominant *BicD* alleles (Fig 3E, F and Fig S3A, B). At least one of these mutations ($BicD^{1}$) appears to suppress the autoinhibited state of BicD in which the dynein and Egl binding sites are folded back on one another (Liu et al. 2013). Antagonism between BicD and Staufen is further supported by the observation that reducing *staufen* gene dosage enhances embryonic lethality associated with the dominant *BicD* alleles (Navarro et al., 2004). Collectively, our genetic interaction experiments indicate a mutually antagonistic relationship between Staufen and Egl, as well as its binding partner, BicD, in the localization of *oskar* mRNA in mid-oogenesis.

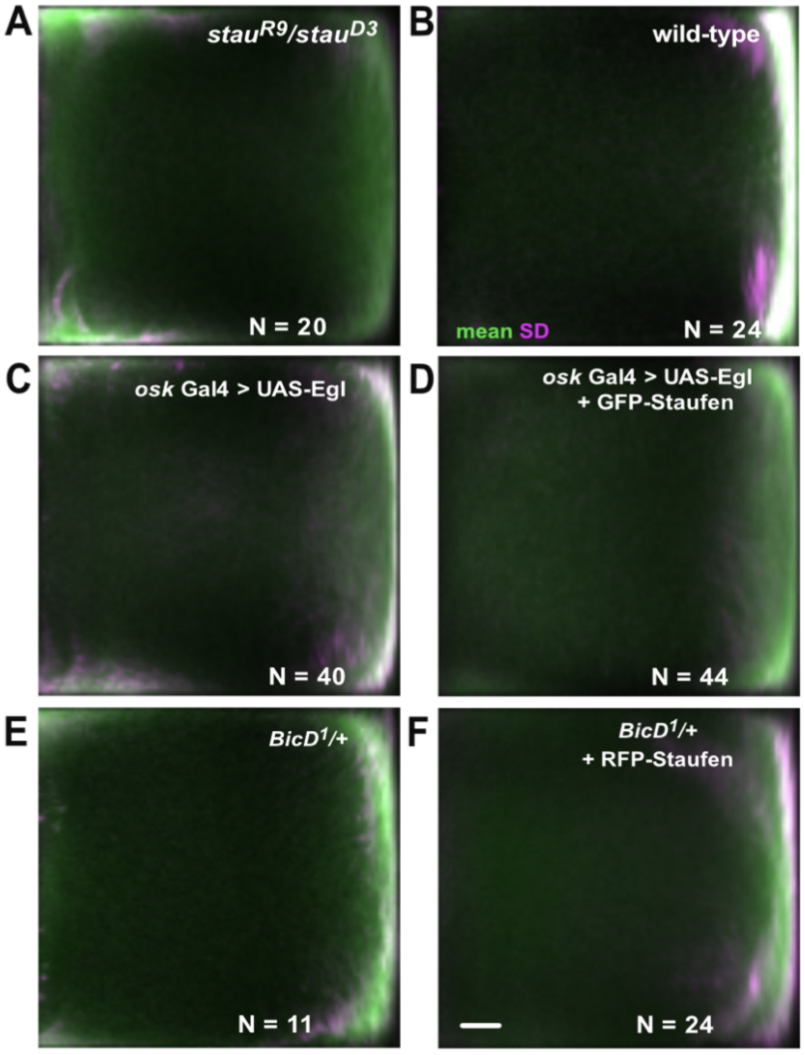

Figure 3: Mutual interference of Staufen and Egl during localization of *oskar* mRNA. (A-F) Average distribution of *oskar* mRNA (green) and variability of its distribution (SD, magenta) in stage 9 oocytes (anterior to the left, posterior to the right). Besides the normal posterior localization of *oskar*, a pronounced anterior accumulation is observed in oocytes that lack Staufen protein (A), overexpress Egl (C) or are heterozygous for one copy of the dominant $BicD^1$ allele (E). Such anterior accumulation of *oskar* is not observed in wild-type oocytes (B), upon Staufen overexpression in Egl-overexpressing oocytes (D), or in $BicD^1$/+ oocytes (F). N indicates the number of oocytes analyzed. Scale bar represents 10% of anteroposterior axis length.

Staufen dissociates Egl from *oskar* mRNPs in the oocyte

To shed light on how Staufen and Egl influence each other *in vivo*, we examined the association of each protein with *oskar* mRNA using smFISH in combination with transgenically expressed fluorescently tagged proteins (Gáspár et al. 2017; Heber et al. 2019).

DIstribution of transgenic Staufen-GFP, expressed by the *stau* promoter close to the endogenous levels (Fig S1I) resembles that of the endogenous protein (St Johnston et al. 1991), and this molecule is functional during *oskar* localization (Fig S1D, E and G). In the oocyte, Staufen-GFP and *oskar* mRNA frequently overlapped. In the nurse cells, there was

little overlap between Staufen-GFP and *oskar*, as previously reported (Little et al., 2015), and only low levels of Staufen-GFP signal were observed, regardless of the developmental stage of the egg-chamber (Fig 4A, A' and B). In the oocyte, the fraction of Staufen-associated *oskar* RNPs in the oocyte increased as a function of their *oskar* mRNA content (Fig S4A). This increase was substantially more pronounced during stage 9 than in earlier stages of oogenesis (Fig 4B). During stage 9, not only the likelihood of Staufen association with *oskar* RNPs increased; the relative levels of Staufen per RNP were also higher than in the preceding stages (Fig 4B'). We previously observed the same behavior for overexpressed Staufen and mammalian Stau2 (Heber et al., 2019). Notably, however, no or greatly reduced scaling of the Staufen signal with *oskar* mRNA content of the mRNPs was observed in the oocyte prior to the onset of *oskar* localization to the posterior (Fig 4B'). This is likely due to limited availability of the protein, as suggested by the relatively low fluorescent signal in early stage Staufen-GFP oocytes (Fig S4G). Collectively, our analysis shows that Staufen preferentially associates with *oskar* RNA in the oocyte and that this association is largely governed by the RNA content of the mRNPs and the spatiotemporal availability of Staufen.

During the same stages of oogenesis, Egl-GFP (which was mildly overexpressed with the α-tubulin84B promoter (Dienstbier et al., 2009)) is abundant in both the nurse cells and the oocyte (Fig 4C and C'). This matches the distribution of endogenous Egl protein, as revealed by immunostaining (Mach and Lehmann, 1997). Colocalization analysis showed that, in contrast to Staufen-GFP, Egl-GFP is already associated with *oskar* mRNPs in the nurse cells (Fig 4D) and maintains its association with *oskar* in the oocyte until the onset of posterior localization. However, from stage 9 onward, we detected no significant colocalization between Egl and mRNPs containing four or more copies of *oskar* mRNA (Fig 4D). In fact, the amount of Egl signal associated with the RNPs increased proportionately with *oskar* mRNA content during early oogenesis, but reduced by about two-fold and became independent of *oskar* mRNA copy number during stage 9 (Fig S4D'). As this loss of Egl from *oskar* mRNPs was an unexpected finding, we wondered if it was caused by the dilution of Egl-GFP by endogenous, untagged Egl. When tested, however, we found that this reduction was robust to changes in the dosage of the Egl-GFP transgene or endogenous unlabelled Egl and was also observed when no unlabeled Egl (egl^1/egl^2 rescued by the Egl-GFP transgene) was present in the oocyte (Fig S4F'). Collectively, these results indicate that whereas Staufen levels increase on *oskar* mRNPs as posterior-ward movement in the oocyte is initiated, there is a concomitant decrease in Egl levels on these structures.

The opposing trends of Staufen and Egl association with *oskar* mRNPs in nurse cells and oocyte (Fig 4B,B' and D,D'), and the increasing concentrations of Staufen in the ooplasm prior to the onset of *oskar* localization (Fig S4G) are consistent with Staufen inhibiting Egl association with *oskar* RNPs in the oocyte. To test this notion, we analyzed the association of Egl-GFP with *oskar* mRNPs in *staufen* mutants. When Staufen protein was absent or greatly reduced, Egl remained associated with *oskar* mRNPs in stage 9 oocytes, and the relative amount of Egl signal that colocalized with the RNPs increased with *oskar* mRNA content (Fig 4E, E' and Fig S4 E, E'). Conversely, when Staufen was mildly overexpressed by RFP-Staufen, the amount of Egl associated with *oskar* RNPs (in particular with those containing 4+ copies of RNA) in the oocyte decreased (Fig 4F, F').

To test biochemically whether Staufen impairs the association of Egl with *oskar* mRNPs *in vivo*, we performed UV crosslinking and GFP immunoprecipitation followed by quantitative

PCR on egg-chambers co-expressing Egl-GFP and either *staufen* RNAi or a control RNAi (*white*) in the germline (Fig 3G, Fig S4H). Substantially more *oskar* mRNA was co-immunoprecipitated with Egl-GFP from extracts of egg-chambers expressing *staufen* RNAi compared to the control (Fig 3G). We conclude from these experiments that Staufen antagonizes the association of Egl with *oskar* mRNA *in vivo*.

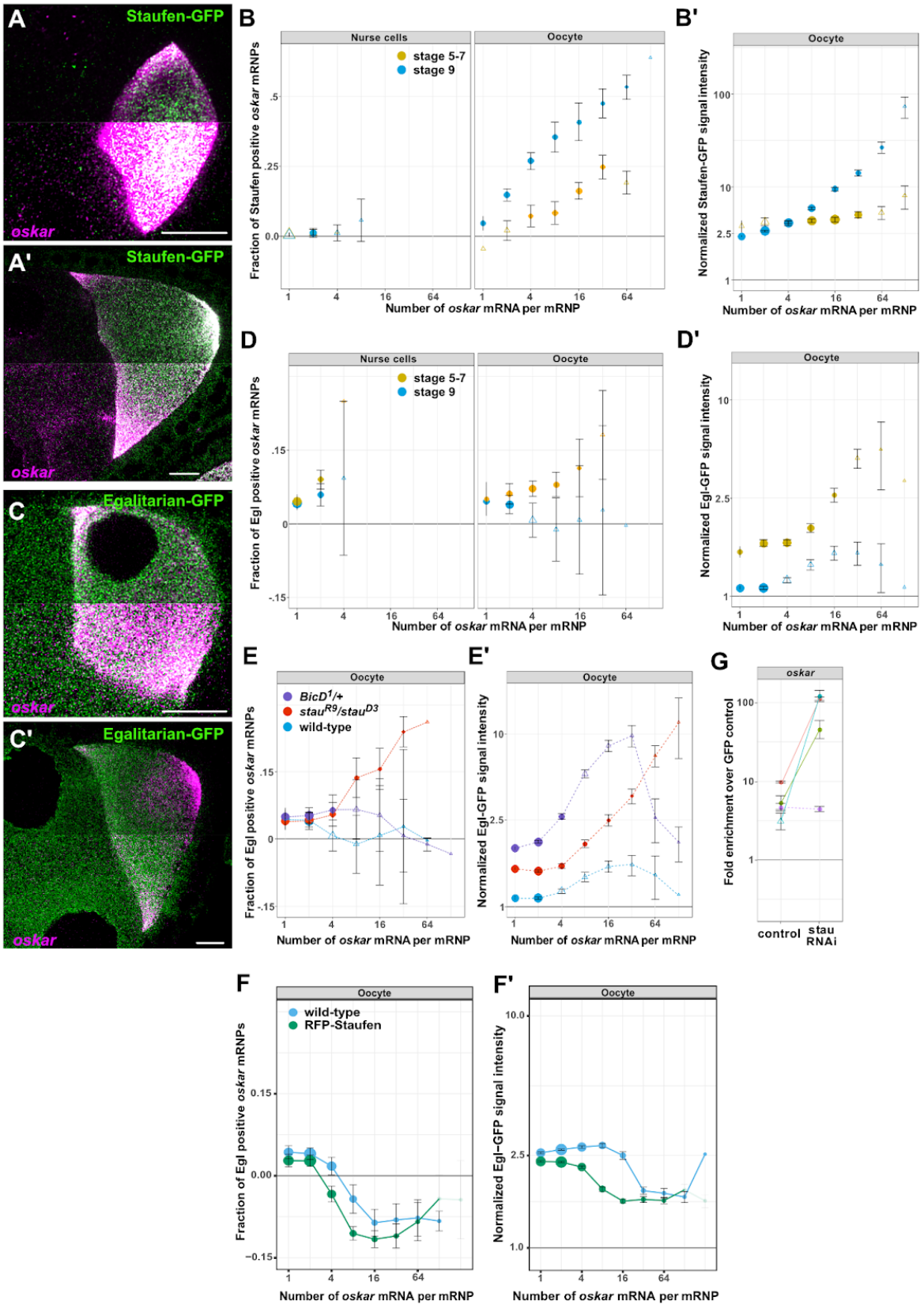

Figure 4: Staufen interferes with association of Egl with *oskar* mRNPs in the oocyte.
(A-A') Distribution of Staufen-GFP (green) prior to (stage 6-7, A) and during (stage 9, A') the posterior localization of *oskar* mRNA (magenta). (B-B') Association of Staufen-GFP with *oskar* mRNPs before (yellow) and during (blue) the posterior localization of *oskar* mRNA. (A-B') Endogenous Staufen was absent

(*stau*^{R9}/*stau*^{D3}). (C-C') Distribution of Egl-GFP (green) before (stage 7, C) and during (stage 9, C') the posterior localization of *oskar* mRNA (magenta). (A, A', C and C') Lower half of panels shown with different brightness/contrast settings to allow appreciation of the signal in the nurse cells. Scale bars represent 10 µm. (D-D') Association of Egl-GFP with *oskar* mRNPs before (yellow) and during (blue) the posterior localization of *oskar* mRNA. (E-E') Association of Egl-GFP with *oskar* mRNPs during stage 9 in the presence (blue) or in the absence (red) of Staufen, or in presence of the dominant *BicD*^{1} mutation (magenta) in the oocyte. (F-F') Association of Egl-GFP with *oskar* mRNPs in stage 9 oocytes upon mild overexpression of Staufen. (C-F') Endogenous, unlabeled Egl was present. (B, D-F) The fraction of Staufen-GFP (B) or Egl-GFP (D-F) positive *oskar* mRNPs as a function of the mRNA content of the RNPs in the nurse cells and in the oocyte. (B', D'-F') Normalized Staufen-GFP (B') or Egl-GFP (D'-F') signal intensity as function of *oskar* mRNA content in the mRNPs. (B, B', D-F') Error bars represent 95% confidence intervals; the size of the circles is proportional to the relative abundance of the given sized *oskar* mRNPs within the entire sample analyzed. (G) Fold-enrichment of two Egl target mRNAs, *oskar* and *bicoid*, in RNA pulldown experiments using Egl-GFP as a bait, in the presence (control) or in the absence of Staufen (*stau* RNAi). Different colors represent different experiments. Paired data are connected with solid ($p<0.05$) or dashed lines ($p>0.05$), indicating significance as determined in pairwise Student's t-test. Empty triangles indicate non-significant enrichment ($p>0.05$) relative to the GFP control. Error bars show standard deviation.

Aberrant anterior localization of *oskar* mRNA correlates with increased Egl association

As described above, BicD is a direct binding partner of Egl, and contacts the dynein and dynactin complexes (Liu et al. 2013; Vazquez-Pianzola et al. 2017; Dienstbier et al. 2009; McClintock et al. 2018; Sladewski et al. 2018). To gain further insight into how the association of Egl influences trafficking of *oskar* mRNA, we examined the effect of the two gain-of-function *BicD* mutations. Both alleles caused an increase in the association of Egl-GFP with mid- to large-sized (4-16 RNA copies) *oskar* mRNPs in stage 9 oocytes when compared to the wild-type control (Fig 4E, E' and Fig S4F, F'). Although the extent of Egl association differed between the two alleles, in both cases the amount of Egl associated with the mRNPs scaled with *oskar* RNA copy number up to 32 copies, in contrast with the low amount of Egl detected on all *oskar* mRNPs in wild-type stage 9 egg-chambers (Fig 4E' and Fig S4F'). Thus, there is a correlation between the ability of the BicD gain-of-function alleles to misdirect *oskar* RNPs to the anterior of the oocyte and their effects on Egl recruitment to these structures in the oocyte cytoplasm.

We reasoned that the anterior localization of *oskar* mRNA in the oocyte observed when untagged Egl is strongly overexpressed (Fig 3C) might be due to an aberrant, concentration-dependent retention of the protein on the mRNPs. To test this idea, we introduced the moderately overexpressed Egl-GFP transgene (Dienstbier et al. 2009) into egg-chambers overexpressing untagged Egl under UAS-Gal4 control. We observed numerous large RNP granules containing high amounts of Egl-GFP (which presumably also contain unlabelled Egl) and *oskar* mRNA (Fig 5A and A') in the nurse cells and at the anterior cortex of the oocyte. Such RNPs were seldom detected in the absence of UAS/Gal4-mediated Egl overexpression (Fig 5A and E). Quantification of the association of Egl with *oskar* showed that when the protein was overexpressed with the UAS/Gal4 system, the relative Egl-GFP signal scaled with *oskar* RNA content in the mRNPs (Fig 5C'). The effect was similar to that observed in the absence of Staufen, and in egg-chambers with BicD gain-of-function alleles (Fig 4E' and S4F'). On the other hand, we found no significant change in Staufen association with *oskar* mRNPs in stage 9 oocytes strongly overexpressing Egl (Fig 5D and D'). This finding indicates that Egl does not interfere with the loading of Staufen on *oskar* mRNPs. However, an abnormal proportion of high copy number *oskar*

mRNPs (10+ times more than in wild type) failed to leave the vicinity of the anterior pole (Fig 4E) when Egl was strongly overexpressed, consistent with our earlier finding that Egl antagonizes Staufen's function in promoting posterior localization of *oskar* mRNA.

Taken together, these data reveal that a common feature of *oskar* mislocalization to the anterior in the absence of Staufen, upon Egl overexpression, and in gain-of-function *BicD* mutants is the failure to release Egl from the RNPs during mid-oogenesis. Our data indicates that this release is mediated by Staufen, which interferes with the association of Egl with *oskar* mRNPs, especially those with high *oskar* mRNA content.

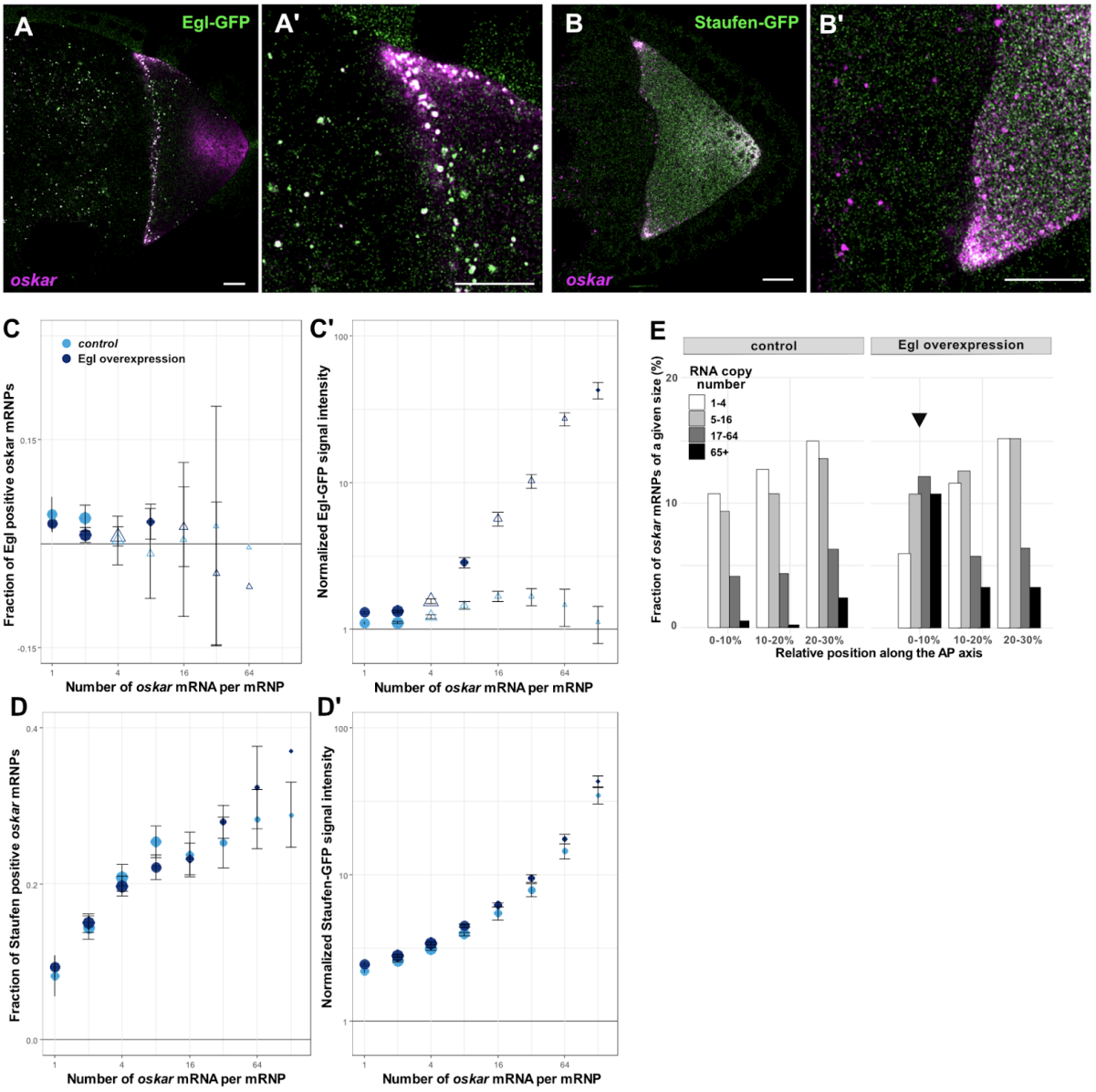

Figure 5: Effect of Egl overexpression on *oskar* mRNP localization and composition.
(A-B') Stage 9 egg-chambers overexpressing Egl in the germline (see Materials and Methods). The *UASp-Egl* transgene is under the control of the *oskar-Gal4* driver. Large RNPs containing *oskar* mRNA are observed in the nurse cells and in the oocyte, near the anterior. These RNPs colocalize with Egl-GFP, expressed from a

single copy of a transgene by the α-tubulin promoter (A, A'). In the case of Staufen-GFP, expressed from a single copy of transgene, no or moderate colocalization in the nurse cells and at the anterior of the oocyte, respectively, is observed (B, B'). Scale bar represents 10 microns. (C-D') Fraction (C, D) of GFP positive *oskar* mRNPs and relative levels of Egl-GFP (C') and Staufen-GFP (D') associated with *oskar* mRNPs as a function of the RNA copy number. Error bars represent 95% confidence intervals, the size of the circles is proportional to the relative abundance of the given sized *oskar* mRNPs within the entire sample analyzed. (E) Relative distribution of *oskar* mRNPs grouped by RNA content along the first 30% of anteroposterior axis. In the wild-type control, less than 1% of large (65+ copies) *oskar* mRNPs are close to the oocyte anterior (first bin). When Egl is overexpressed, around 10% of such large *oskar* mRNPs are present close to the oocyte anterior (first bin, arrow), while the rest of the oocyte has almost identical distribution of *oskar* mRNPs to control (Fig S5A)

Dissociation of Egl affects dynein function but does not prevent association of the motor with *oskar* mRNPs

As described above, Egl functions as an adaptor molecule linking mRNA localization signals to dynein-dynactin (Amrute-Nayak and Bullock, 2012; Dienstbier et al., 2009; Navarro et al., 2004). However, it has been proposed that Egl is not the only means to link the motor complex to RNPs. In *ex vivo* experiments, both the *K10* and *hairy* mRNAs recruited some dynein-dynactin complexes through Egl-BicD, and others through an Egl-BicD independent mechanism, which presumably involved other RBP linkers or direct interactions between the RNA and the motor complex (Bullock et al. 2006; Amrute-Nayak, 2012; Dix et al., 2013; Soundararajan and Bullock, 2014). Only those dynein-dynactin complexes interacting with Egl-BicD were capable of long-distance transport, explaining how these two adaptors promote minus-end-directed trafficking of mRNAs. However, how Egl influences dynein recruitment to RNPs has not been examined *in vivo*.

To address this question, we examined the association of *oskar* mRNA (detected by smFISH) with fluorescently tagged versions of p50/Dynamitin, a dynactin subunit, BicD and Dynein heavy chain (Dhc) in the nurse cells and oocyte. We saw little difference in association of either protein with *oskar* mRNA between the stage 9 nurse cells and oocyte (Fig. 6A-D). This contrasts with the situation for Egl, which showed a relative reduction in association with *oskar* in the stage 9 oocyte (Fig. 4D and D'). The fraction of *oskar* mRNPs associated with BicD and the dynein-dynactin subunits also did not change as a function of RNA content in the oocyte (Fig 6D). Notably, the relative amount of these proteins associated with *oskar* mRNPs in the oocyte was approximately double that in the nurse cells (Fig 6E). The amount of BicD and p50 associated with the mRNPs in the oocyte was independent of *oskar* copy number, whereas Dhc association increased as a function of *oskar* mRNA content (Fig 6E). This result suggests that Dhc and BicD/p50 are not recruited to *oskar* mRNPs by identical mechanisms.

Increased levels of Egl on *oskar* mRNPs in the absence of Staufen (Fig 4E, E' and S4E, E') or in the presence of excess Egl (Fig 5D, D') could in principle result in increased recruitment of the dynein motor. However, when we analyzed GFP-Dhc association with *oskar* mRNPs, we found no major difference between *staufen* RNAi, Egl-overexpressing, and control oocytes (Fig 6F and F'). These data indicate that Egl is not obligatory for recruitment of dynein-dynactin to a native cargo *in vivo*. Intriguingly, *staufen* RNAi and Egl overexpressing oocytes also did not display an increase in the association of BicD with *oskar* RNPs (Fig 6G and G'). Thus, there appears to be an Egl-independent mechanism for recruiting BicD to these structures.

The loss of Egl from larger *oskar* mRNPs during stage 9 suggests that dynein – although present – is not fully active. To test if this is the case, we stratified our *ex vivo oskar* motility data on the basis of relative *oskar* MCP-GFP fluorescence intensity (Video S1 and S2), as we have previously shown that RNPs with a greater RNA content have less Egl bound (Fig 4D'). Although the lack of a nurse cell reference in the assay (Little et al., 2015) and the stochastic nature of the MCP-MS2 interaction (Wu et al., 2012) precluded quantification of absolute mRNA copy numbers, classification of relative RNA signal revealed that whereas around 35-40% of small *oskar* mRNPs moved towards the microtubule minus ends, fewer than 20% of larger *oskar* mRNPs were minus end-directed. Hence, the dominance of plus end-directed runs increased from around 2-fold for small (1-2 relative units), to around 3.5-fold for larger (3 or more units) *oskar* mRNPs (Fig 6H). In summary, in stage 9 oocytes, *oskar* RNPs lacking Egl maintain their association with the dynein machinery but are defective in minus-end-directed motion.

Interestingly, *ex vivo* motility analysis revealed that knockdown of Staufen strongly reduces the proportion of transported *oskar* mRNPs that are large (~15%, 95/624 for control versus <1%, 4/460 for *stau* RNAi, Fig 6H), although it has no effect on the oligomerization state of *oskar* (Fig S4B). While it is unclear why the larger *oskar* mRNPs are less likely to undergo directed transport when Staufen is depleted, this observation can explain the paucity of *oskar* mRNA transport detected in live *staufen* mutant oocytes when using the less sensitive confocal live-cell imaging technique (compare Video S2 and S4; Zimyanin et al., 2008).

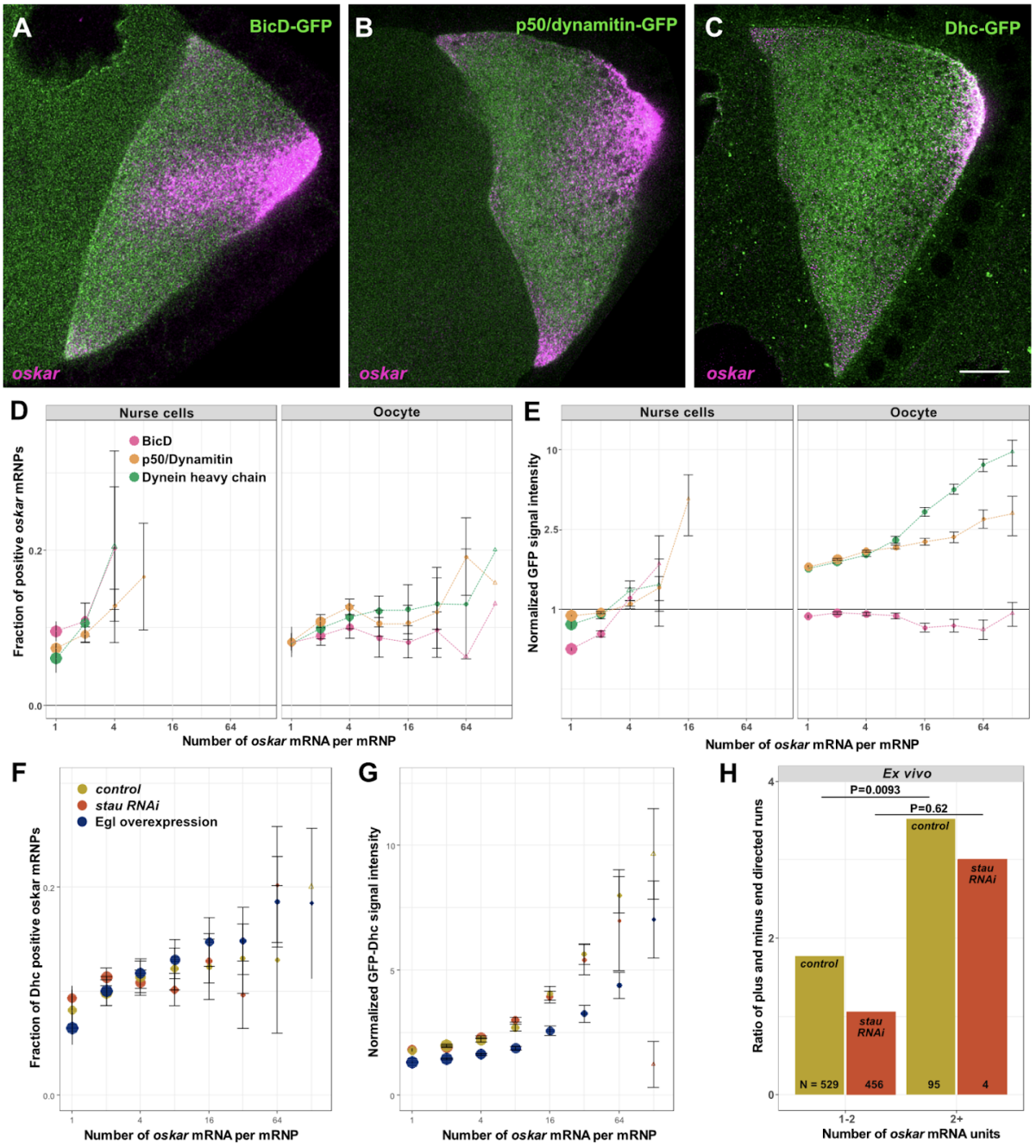

Figure 6: Recruitment of the dynein machinery during the transport of *oskar* mRNPs.
(A-C) Localization of BicD (green, A), p50/dynamitin (green, B) and Dhc (green, C) in egg-chambers during mid-oogenesis. *oskar* mRNA is shown in magenta. Scale bar represents 10 µm. (D) Fraction of *oskar* mRNPs colocalizing with BicD (magenta), p50/dynamitin (orange) and Dhc (green) in the nurse cells and in the oocyte; mRNPs classified according to *oskar* mRNA copy number. (E) Normalized GFP signal intensity of BicD (magenta), p50/dynamitin (orange) and Dynein heavy chain (green) colocalizing with *oskar* mRNPs. (F) Fraction of GFP-Dhc positive *oskar* mRNPs and (G) GFP-Dhc amounts on *oskar* mRNPs when Staufen levels are reduced (red) and in the presence of excess Egl (dark blue). (H) Dominance of plus end-directed transport over minus end-directed transport of *oskar-MS2(10x)* mRNPs ex vivo as a function of normalized MCP-GFP signal in control (brown) and *staufen* RNAi (red). *oskar* mRNPs are clustered into small (1-2 normalized units) and large (3 or more units) categories based on MCP-GFP signal intensity. P-values of pairwise Fisher-exact tests are shown. Number of analyzed motile *oskar* mRNPs is indicated.

Staufen activity is controlled by Egl-mediated delivery of its mRNA into the oocyte

As shown above, proper *oskar* localization to the posterior pole depends on availability of Staufen protein in stage 9 oocytes. However, it is unclear how spatio-temporal restriction of Staufen is brought about during development. We noticed that only trace amounts of Staufen-GFP accumulated in the early arrested oocyte primordium in *egl* mutant egg-chambers (Fig 7A-C). This observation raised the possibility that Egl mediates the enrichment of Staufen into the ooplasm of wild-type egg-chambers. The normal ooplasmic accumulation of Staufen could in principle result from its transport in association with target mRNAs from the nurse cells into the oocyte. However, this seems unlikely, as we detected no association of Staufen-GFP with its main target, *oskar* mRNA, in the nurse cells (Fig 4A-B'), and both Staufen and Staufen-GFP signal accumulated in the oocyte even in the absence of *oskar* mRNA (Fig S6A-C). Alternatively, *staufen* mRNA might be transported into and translated within the oocyte. Whereas *staufen* mRNA was enriched during early oogenesis in small oocytes expressing control RNAi (Fig 7F-G), we observed no such enrichment in egg-chambers in which *egl* was partially knocked down by RNAi (Fig 7E, E' and G). Furthermore, while *staufen* mRNA did not display any specific localization pattern in the ooplasm of wild-type oocytes (Fig 7H), upon Egl overexpression it was enriched at the anterior pole of the oocyte (Fig 7H'). This observation suggests that, similar to other oocyte-enriched transcripts, such as *oskar*, *gurken* and *bicoid* (Ephrussi et al., 1991; Berleth et al., 1988; Neuman-Silberberg and Schüpbach, 1993; see also Fig 6), *staufen* mRNA is a target of Egl-dependent transport by dynein.

Colocalization analysis revealed that *staufen* mRNA and Egl-GFP are associated in the germline, and that this association is significantly lower in the oocyte than in the nurse cells (Fig 7I). We also detected Staufen protein in association with *staufen* mRNPs in stage 9 oocytes (Fig 7J), as we previously observed for *oskar* mRNPs (Fig 4). Taken together, these data indicate that the Egl-dependent transport of *staufen* mRNA into the oocyte by dynein underlies ooplasmic Staufen enrichment, which in turn inactivates the machinery for minus end-directed transport of *oskar* (and likely *staufen*) mRNPs in the stage 9 oocytes. This constitutes a feed-forward mode of regulation, whereby the dynein transporter system ensures the localized production of its inhibitor, leading to its own inactivation. This predefined program thereby allows kinesin-1-dependent delivery of *oskar* mRNA to the oocyte posterior.

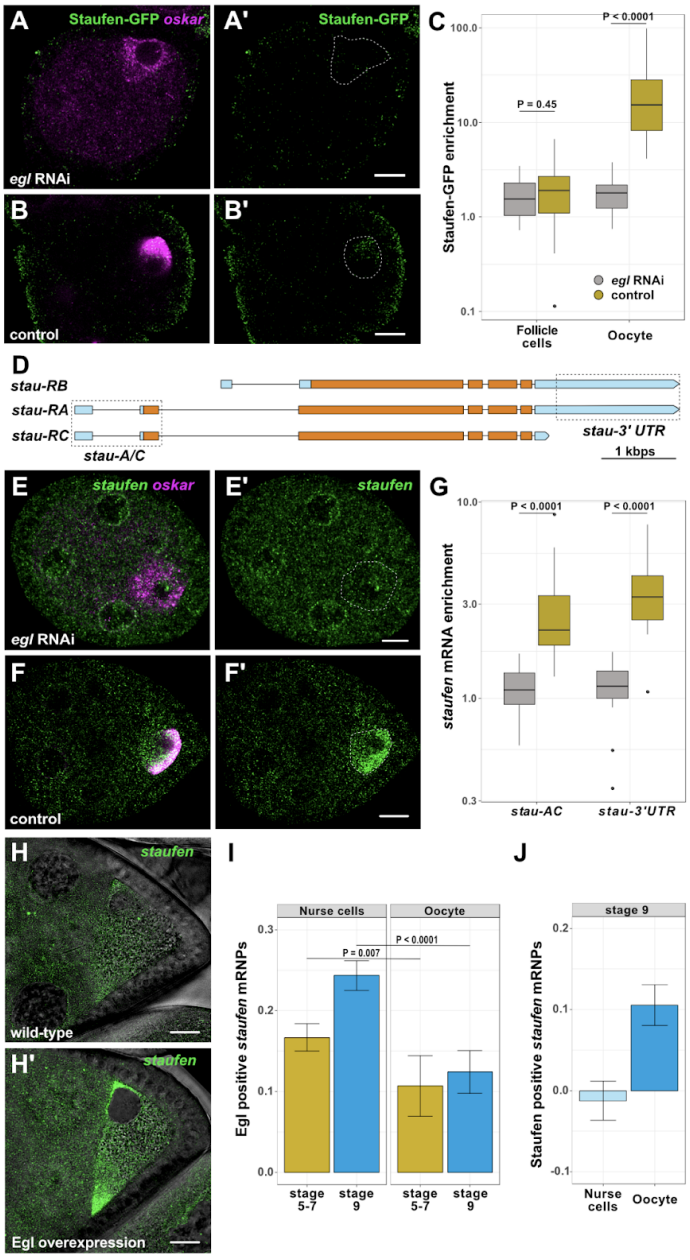

Figure 7: Egl promotes enrichment of Staufen mRNA and protein in the ooplasm
(A-B') Staufen protein expression detected via Staufen-GFP (green) in early stage egg-chambers expressing *egl* (A, A') or control RNAi (B, B'). (C) Enrichment of Staufen-GFP signal in oocytes expressing *egl* (grey) or control RNAi (brown) relative to the sibling nurse cells. Enrichment of Staufen-GFP in somatic follicle cells - which do not express the shRNA is used as a control. P-values of pairwise Student's t-test are shown. (D) The three RNA isoforms encoded by the *stau* locus. Regions targeted by the stau-A/C and the stau 3'UTR probe sets are indicated by dashed boxes. (E-F') Localization of *staufen* mRNA, detected by the *stau-A/C* isoform specific probe set, in early egg-chambers expressing *egl* RNAi (E, E') or control RNAi (F, F'). *oskar* mRNA (magenta A, B, E and F) was used to identify the oocyte, which is indicated by a dashed outline in A', B', E' and F'. (G) Enrichment of *staufen* mRNA - detected by the *stau-A/C* isoform specific or the long *stau 3'UTR* specific probe set. (H, H') Localization of *staufen* mRNA (green, detected by the stau A/C probe set) in wild-type and Egl-overexpressing stage 8 oocytes. (I, J) Fraction of *staufen* RNPs (detected by the stau A/C probe set) associating with (I) Egl in the nurse cells and in the oocyte, and (J) with Staufen in the oocyte. Scale bars represent 10 µm.

Discussion

The activity of motor molecules is essential for establishing proper localization of mRNA molecules, which in turn underlies spatiotemporal restriction of protein function (Abouward and Schiavo, 2021; Martin and Ephrussi, 2009; Mofatteh and Bullock, 2017; St Johnston, 2005). The dynein and kinesin microtubule motors play key roles in positioning of mRNAs in many systems, including by acting sequentially on the same RNP species (Mofatteh and Bullock 2017; Turner-Bridger et al. 2018; Gagnon et al. 2013; Baumann et al. 2012). However, it is unclear how the opposing activities of these motors are coordinated during RNP trafficking.

Here we use the tractable *Drosophila* egg-chamber to reveal a mechanism for spatiotemporal control of dynein and kinesin-1 activity. Central to this system are two dsRBPs, Staufen and Egl. Several genetic studies have shown previously that these proteins have opposing activities in the context of *oskar* mRNA localization in the oocyte and anteroposterior patterning (Navarro et al. 2004; Mohler and Wieschaus, 1986) and both proteins were shown to form a complex with *oskar* (Sanghavi et al. 2016; Laver et al. 2013). Recent work by Mohr and colleagues (Mohr et al. 2021), which was published while this manuscript was in preparation, further corroborated the *in vivo* interference between Staufen and Egl. These authors also investigated the interplay between these proteins *in vitro* with RNA binding assays. It was shown that *in vitro* Egl binds to a truncated version of stem-loop 2 in the *oskar* 3' UTR (SL2, Jambor et al., 2014) termed the Transport and Anchoring Signal (TAS) (Mohr et al., 2021). The TAS partially overlaps with one of the Staufen Recognized Structures (SRS; Laver et al., 2013), which are important for Staufen binding *in vitro* and for proper *oskar* mRNA localization *in vivo* (Mohr et al., 2021). These data suggest that Staufen could antagonize Egl function by directly interfering with binding of the latter protein to *oskar* mRNA. Supporting this idea, we found that knocking down Staufen increases the biochemical association of Egl with the mRNA. The results of our *in vitro* motility assays are also consistent with Staufen reducing the association of Egl with *oskar* mRNA, as RNA binding to Egl is a prerequisite for full dynein activity within this minimal RNP (Sladewski et al. 2018; McClintock et al. 2018)).

Our study additionally reveals through smFISH-based colocalization analysis of egg-chambers how the interactions of Staufen and Egl with *oskar* mRNA are orchestrated in time and space. When Staufen levels are low, such as in early oogenesis, amounts of Egl per RNP scale with *oskar* RNA content. During stage 9, this scaling is lost in the oocyte and the relative amount of Egl on *oskar* mRNPs decreases as Staufen is recruited to *oskar*. Our data indicate that Staufen-mediated displacement of Egl is a critical step in switching to kinesin-1-based trafficking of *oskar* mRNA to the posterior pole. This switch is also likely to involve the activities of exon junction complex components, which are required for posterior localization of *oskar* (van Eeden et al. 2001; Zimyanin et al. 2008; Palacios et al. 2004; Mohr et al. 2001; Newmark and Boswell 1994; Hachet and Ephrussi 2004; Hachet and Ephrussi 2001; Ghosh et al. 2012). Our study provides a framework for understanding how the activities of these factors are coordinated with that of Staufen.

Intriguingly, whilst an excess of Staufen can dissociate Egl from *oskar* RNPs, increasing Egl concentration does not overtly affect Staufen recruitment with these structures. This observation might be due to the five-to-one excess of SRSs over the TAS in each *oskar* molecule (Mohr et al., 2021), which could mask the loss of Staufen binding to the TAS-proximal SRS.

We also found that dissociation of Egl from *oskar* mRNPs in the stage 9 oocyte does not detectably alter the amount of dynein on these structures. This work lends *in vivo* support to the notion that additional proteins or RNA sequences can recruit dynein and dynactin in an inactive state to RNPs (Bullock et al. 2006; Amrute-Nayak, 2012; Dix et al., 2013; Soundararajan and Bullock, 2014). Presumably, Egl recruits only a small fraction of the total number of dynein complexes on *oskar* mRNPs or activates the motility of complexes that are also linked to the RNA by other factors. Unexpectedly, we reveal that the bulk association of BicD with *oskar* RNPs is also not dependent on Egl, pointing to an additional mechanism for recruiting BicD, presumably in the autoinhibited state that prevents dynein activation (Liu et al. 2013; Hoogenraad et al. 2003). While the relative amount of the dynein machinery associated with *oskar* RNPs is greater in the oocyte than the nurse cells, dynein's association with *oskar* RNPs in the oocyte does not scale with RNA content. How the amount of dynein recruited to these RNPs could be limited is unclear but this mechanism could be a means to prevent sequestration of this multi-functional motor to a very abundant cargo (~0.5-1 million copies of *oskar* mRNA per oocyte (Little et al. 2015)).

A key question raised by our analysis of Staufen's effects on motor switching is how the timing and location of this process is controlled. We provide evidence that this key aspect of *oskar* mRNA localization is based on another mRNA localization process. Egl is part of s*taufen* mRNPs and is responsible for the enrichment of *staufen* mRNA in the developing oocyte. We propose this mechanism constitutes a feed-forward type of switch, whereby the activity of the dynein-mediated transport machinery deploys its own negative regulator to a distant location. The resultant increase in levels of ooplasmic Staufen levels in the ooplasm prevents dynein-mediated transport of *oskar* to the anterior of the oocyte, while the almost complete absence of the protein from the nurse cells is likely to be important for uninterrupted transport of *oskar* RNPs into the oocyte by dynein during early- and mid-oogenesis. Staufen protein might also modulate its own localization in the ooplasm by antagonizing the association of *staufen* mRNA with Egl, and thereby its minus end-directed motility. Consistent with this notion, the level of Egl on *staufen* RNPs declines at a stage similar to when Staufen inhibits the association of Egl with *oskar* RNPs. As Staufen controls localization and translation of other mRNAs in the maturing oocyte (Ferrandon et al. 1994; St Johnston et al. 1991), mRNA-based regulation of the protein distribution in the egg-chamber is likely to have functions that extend beyond orchestrating *oskar* mRNA localization.

Given that the function of Staufen is conserved (Heber et al., 2019), it is plausible that the feed-forward loop established by *staufen* RNA localization during *Drosophila* oogenesis is an evolutionarily conserved process that controls RNA targeting and protein expression in other tissues and organisms. Consistent with this idea, localization of the mRNAs encoding mammalian Staufen proteins have been observed in the dendrites of mammalian hippocampal neurons (Cajigas et al. 2012) (Middleton et al. 2019). As SRSs are numerous in transcriptomes of many organisms, including humans (Laver et al. 2013), such a mechanism could spatiotemporally regulate a wide range of post-transcriptional events. This

regulation could involve antagonism of a large number of RBPs whose binding sites overlap with SRSs.

Methods

Fly strains

To knock down *staufen* and *egl* RNA levels, we used the P{TRiP.GL01531} (FBal0281234) and the P{TRiP.HM05180} (FBal0240309) transgenic lines. TRiP line against the *w* gene (P{TRiP.GL00094} - FBal0262579) was used as a negative control. The following mutant lines were used to disrupt or modify gene function: *stau*[D3] (FBal0016165) and *stau*[R9] (FBal0032815) alleles in heterozygous combination; *egl*[1] (FBal0003574) and *egl*[2] (FBal0003575); BicD[1] (FBal0001140) and BicD[2] (FBal0001141); *osk*[A87] (FBal0141009) in combination with *Df(3R)p-XT103* (FBab0002842) to remove *oskar* mRNA from egg-chambers. w[1118] (FBal0018186) was used as the wild-type control.
To overexpress Staufen, we used the αTub67C:GFPm6-Staufen (FBal0091177), αTub67C:RFP-Staufen (Zimyanin et al., 2008) transgenic lines and a P{UASp-Staufen} transgene inserted onto the 3rd chromosome (kind gift of F. Besse)
To overexpress Egl protein, we used the P{UASp-egl.B} transgene (FBtp0022425) inserted on the X or the 3rd chromosome.
To label proteins of interest, we used the following fluorescently tagged reporter lines: P{Staufen-GFP} inserted on the 3rd chromosome, expressing Staufen-GFP under control of the endogenous *stau* promoter (kind gift of F. Besse); P{tub-egl.EGFP} (FBtp0041299) inserted on the 3rd chromosome, driving expression of Egl-GFP ; P{UASp-BicD.eGFP} (FBtp0069955) and P{UAS-DCTN2-p50::GFP} (FBtp0016940) transgenic insertions to label BicD and Dynamitin, respectively. To drive the expression of the TRiP RNAi lines and other UASp constructs in the female germline, one copy of P{oskar-Gal4} (FBtp0083699) was used. For moderate overexpression of UASp-GFP-Staufen, we used one copy of P{matα4-GAL-VP16} (FBtp0009293)

The Dhc locus (Dhc64C) was tagged with the EmeraldGFP coding sequence to generate a GFP-Dhc expressing fly line according to protocols of the flyCRISPR website ((Gratz et al., 2013) O'Connor-Giles et al., 2014; https://flycrispr.org/). The locus was targeted using CRISPR/Cas9 and the following guide RNA (5' GAGTCACCCATGTCCCACAA)). The introduced double-stranded break was repaired by homologous recombination using an in-frame EmeraldGFP coding sequence flanked by two ~ 700 bp long homology arms targeting around the Dhc translation start codon. F1 generation embryos were screened for GFP fluorescence to identify individuals with a modified genome. Flies homozygous for GFP-Dhc are viable and fertile. All stocks were raised on normal cornmeal agar at 25 °C, and females were fed a high protein diet overnight before harvesting their ovaries.

RNA co-immunoprecipitation (RIP) from ovarian lysate

RIP was carried out as described in (Gáspár et al., 2017). Briefly, ovaries from 50 flies were dissected in Brb80 (80 mM PIPES, 1 mM $MgCl_2$, 1 mM EGTA, pH 6.8) and lysed in Pre-XL

buffer (20mM Tris-Cl, 150mM KCl, 4mM $MgCl_2$, 2xPIC, 1mM PMSF, pH7.5; supplemented with 40U of RiboLock RNase Inhibitor per 100µL lysate). Ovaries were ground using a pestle and centrifuged for 1 min at 500 x g. The supernatant was extracted and crosslinked at 0.3J/cm^2. The lysate was equalized with 1 volume of Pre-XL buffer, 1 volume of RIPA (10 mM Tris/Cl pH 7.5; 150 mM NaCl; 0,5 mM EDTA; 0,1% SDS; 1% Triton X-100; 1% Deoxycholate, 0.09% Na-Azide) buffer and 8 volumes of low salt buffer (20mM Tris-Cl, 150mM KCl, 0.5mM EDTA, 1mM PMSF). GFP-Trap®_MA beads were washed with low salt buffer and blocked for 60 mins at room temperature in Casein Blocking Buffer (Sigma-Aldrich) supplemented with 50 µg/mL Heparin. Lysate was incubated with beads for 90 minutes at 4°C. The beads were then washed six times with high salt buffer (20mM Tris-Cl, 500mM NaCl, 1mM EDTA, 0.1%SDS, 0.5mM DTT, 1xPIC, 1mM PMSF) and twice with PBT (PBS + 0.1% Triton). Endogenous RNA cross-linked to bait protein was recovered from the beads using the QuickRNA Microprep Kit (Zymo Research). Complementary DNA was synthesized using the SuperScript III First-Strand Synthesis kit (Invitrogen) and used as template for PCR using *oskar* and *bicoid* primers.

Single molecule fluorescent hybridization (smFISH)

Single molecule FISH was carried out as described previously (Gaspar et al., 2017; Gáspár et al., 2017; Heber et al., 2019). Briefly, ssDNA oligonucleotides complementary to *oskar* (Gaspar et al., 2017) and *staufen* mRNAs (Table S1) were mixed and labelled with Atto532, Atto565 or Atto633 according to the protocol described in Gaspar et al., 2017.
Drosophila ovaries expressing fluorescent reporter transgenes were dissected in 2% v/v PFA, 0.05% Triton X-100 in PBS and fixed for 20 min. The fixative was removed by two 5 minute washes in PBT (PBS + 0.1% (v/v) Triton X-100, pH 7.4). Ovaries were pre-hybridized in 200 µL 2 × HYBEC (300 mM NaCl, 30 mM sodium citrate pH 7.0, 15% (v/v) ethylene carbonate, 1 mM EDTA, 50 µg per mL heparin, 100 µg per mL salmon sperm DNA, 1% (v/v) Triton X-100) for 10 min at 42 °C. Meanwhile, the 50 µL probe mixture (5 nM per individual oligonucleotide) was prepared and pre-warmed to hybridisation temperature. After 10 minutes of pre-hybridization, the probe mix was mixed into the pre-hybridization mixture. After 2 hours of hybridization at 42 °C, the unbound probe molecules were washed out of the specimen by two washes in pre-warmed HYBEC and a final wash in PBT at room temperature. To boost signal intensity for the protein enrichment analysis of Staufen-GFP in early egg-chambers, we incubated the ovaries in GFP-Booster (Chromotek) diluted 1:2000 in PBT for 1 hour, then washed the sample three times for 10 minutes in PBT. Ovaries were mounted in Vectashield and processed for smFISH analysis.

Microscopy and image analysis

All imaging was carried out on a Leica TCS SP8 confocal laser scanning microscope using a 20x dry (NA = 0.75) objective for imaging the RNA distribution in the oocytes and a 63x oil immersion (NA = 1.4) objective for analysis of RNA or Staufen-GFP protein enrichment in early oocytes and for colocalization analysis between RNPs and the fluorescently labelled Staufen and Egalitarian proteins.

RNA distribution analysis

Analysis of *oskar* and *bicoid* mRNA distribution was carried out as described in (Gaspar et al., 2014; Gáspár et al., 2017; Heber et al., 2019). Briefly, we manually defined the outlines of

the oocytes and their anteroposterior (AP) axis, using a custom-made ImageJ plug-in, the smFISH signal was redistributed into a 100 × 100 matrix. Each column of the matrix represents the relative amount of signal found under 1% of the AP axis length, with anterior on the left (column 1) and posterior on the right (column 100). The matrices from different oocytes of the same genotype and stage were averaged to obtain an average view RNA localization. The center-of-mass (relative to the geometric center of the oocyte) was determined and compared statistically using a Kruskal–Wallis test followed by pairwise Mann–Whitney U test against the control.

RNA and protein enrichment analysis

The boundaries of the somatic follicle cells, nurse cells and oocyte were manually defined, and the fluorescence intensity of smFISH or GFP signal in these compartments was measured by ImageJ. The extent of enrichment of RNA and protein in the somatic follicle cells and the oocyte was obtained by normalizing the measured fluorescence intensity values to the corresponding values obtained for the nurse cells.

Colocalization analysis between mRNPs and fluorescent reporters

Analysis was carried out as described in (Gáspár et al., 2017; Heber et al., 2019). Briefly, images for colocalization analysis were deconvolved using Huygens Essential (https://svi.nl) and segmented using a custom ImageJ (Schneider et al. 2012) plug-in. Nearest-neighbor pairs between mRNPs and fluorescent reporters were identified, their position and signal intensities were extracted from the nurse cell and oocyte compartments, excluding any nuclear areas in the field of view. Number of mRNA molecules in an mRNP and normalization of the fluorescent reporter signal was carried out by fitting multiple Gaussian functions to the corresponding signal intensity distributions taken from the nurse cells using the mixtools package in R (Benaglia et al., 2009; R Core Team, 2014). The μ value of Gaussian fit that described the largest portion of the distribution in the nurse cells (almost the lowest value of all fitted μ values) was taken as the signal intensity of one unit (for mRNPs the intensity of a signal mRNA molecule). These unit values were used to normalize raw signal intensities. RNPs were clustered based on this normalized intensity under the following rule: [2i:2i+1], $i \in [0:8]$, i.e., 1, 2:3, 4:7, 8:15, etc. The observed nearest-neighbor colocalization frequencies were computed for each cluster and were compared to the expected colocalization frequencies (governed by the object-densities, determined in randomized object localizations). Similarly, the mean, normalized intensity of colocalizing fluorescent reporter molecules was calculated for each cluster. Correlation between RNA content and the normalized mean fluorescent reporter intensity was tested and compared using least-squares means analysis in R (Lenth, 2016).

Statistical analysis

All statistical analyses performed are indicated in the respective figure legend. All analysis was done using R (R Core Team, 2014) and RStudio (www.rstudio.com). All graphs were plotted by the ggplot2 library in R (Wickham, 2016).

Protein expression, purification, and fluorescent labelling

Recombinant dynein (human), Egl (*Drosophila*), and BicD (*Drosophila*) were expressed, purified, and fluorescently labelled as described previously (McClintock et al. 2018). Briefly, complexes of the complete dynein holoenzyme and of Egl/BicD were expressed in *Sf*9 insect cells and purified by affinity chromatography using ZZ-tags on the dynein heavy chain or Egl. Fluorescent labelling of the dynein heavy chain with SNAP-Cell TMR Star or SNAP-Surface Alexa Fluor 647 via an N-terminal SNAPf tag was performed on-column prior to elution from the IgG affinity resin by cleavage of the ZZ epitope by TEV protease. All complexes were further purified by FPLC-based gel-filtration chromatography, using either TSKgel G4000SWxl (dynein) or Superose 6 Increase 3.2/300 GL (Egl/BicD) columns. The dynactin complex (porcine) was purified natively from pig brains as described previously (Schlager and Hoang et al. 2014, Urnavicius et al .2015). Extracts were clarified and fractionated by FPLC using SP Sepharose (cation exchange, ~250ml bed volume), Mono Q 4.6/100 PE (anion exchange), and TSKgel G4000SW (gel-filtration) columns.
Recombinant Staufen (*Drosophila*) was cloned as fusion protein with an N-terminal His_6-rsEGFP2-tag and a C-terminal His_6-tag in pFastBacDual between the KpnI and HindIII sites and expressed in *Sf*21 insect cells using the Bac-to-Bac expression system (Thermo Fisher). The protein was purified by affinity chromatography on HisTrap FF in 1x PBS + 880 mM NaCl, 400 mM arginine, 10 mM - 200 mM imidazole, 2 mM DTT and HiTrap Heparin HP in 40 mM Bis-Tris pH 7.5, 150 mM NaCl – 1000 mM NaCl, 40 mM arginine, 2 mM DTT and a final gel-filtration on Superdex200 Increase in a final buffer of 40 mM Bis-Tris pH 7.5, 150 mM NaCl, 2 mM DTT.
In all cases, eluted protein was dispensed into single-use aliquots, flash-frozen in liquid nitrogen, and stored at -80°C.

RNA synthesis and purification

The *oskar* RNA used for the reconstitution assay was uncapped and synthesized *in vitro* using the MEGAscript T7 Transcription Kit (Ambion). The RNA was transcribed from a linearized plasmid DNA template containing an ~529-nt region of the *osk* 3'UTR previously defined as region 2+3 that includes the oocyte entry signal (OES) and promotes the localization of reporter transcripts to the developing oocyte (Jambor et al. 2014). For fluorescent labelling of transcripts, Cy5 UTP or Chromatide Alexa Fluor 488 UTP was included in the transcription reaction with a 2-fold or 4-fold excess of unlabelled UTP, yielding transcripts with an average of ~5 or ~14 fluorophores per RNA molecule, respectively. Excess fluorescent UTP was removed using 2 successive rounds of Sephadex G-50 desalting spin columns per transcription reaction. Transcripts were subsequently purified by ammonium acetate/ethanol precipitation and resuspension in nuclease-free water. RNA was dispensed into single-use aliquots and stored at -80°C.

In vitro RNP reconstitution assays

TIRF-based single-molecule reconstitution assays were performed as described previously (McClintock et al. 2018). Briefly, taxol-stabilized porcine microtubules were polymerized with a mixture of unlabelled tubulin, HiLyte 488 tubulin and biotin-conjugated tubulin, and immobilized in imaging flow chambers by streptavidin-based linkages to biotin-PEG passivated cover slips. RNP assay mixes containing relevant combinations of dynein,

dynactin, Egl, BicD, *oskar* RNA, and Staufen were then diluted to concentrations suitable for imaging of single molecules (~2.5 nM for dynein), applied to the flow chamber and subsequently imaged by TIRF microscopy. For assays testing the effect of Staufen on RNA motility, the complexes were assembled for 45-60 minutes on ice with components diluted in GF150 buffer (25 mM HEPES pH 7.3, 150 mM KCl, 1 mM $MgCl_2$, 5 mM DTT, 0.1 mM MgATP, 10% glycerol) to concentrations of 100 nM TMR-dynein, 200 nM dynactin, 500 nM Egl/BicD, and 1 µM *oskar* RNA. This assembly mix was then diluted 1:1 with either ~4 µM rsEGFP2- Staufen or Staufen storage buffer (40 mM Bis-Tris pH 7.5, 150 mM NaCl, 2 mM DTT) and incubated for at least a further 15 minutes on ice. Just prior application to the imaging chamber, this mixture was further diluted 20-fold in Motility Buffer (30 mM HEPES pH 7.3, 50 mM KCl, 5 mM $MgSO_4$, 1 mM EGTA pH 7.3, 1 mM DTT, 0.5 mg ml^{-1} BSA, 1 mg ml^{-1} a-casein, 20 µM taxol) with added MgATP (2.5 mM final concentration) and 1x oxygen scavenging system (1.25 µM glucose oxidase, 140 nM catalase, 71 mM 2-mercaptoethanol, 25 mM glucose final concentrations) to reduce photobleaching. For assays testing the effect of Egl/BicD on RNA binding and motility on microtubules, the complexes were assayed as above except that primary assembly mixes consisted of 100 nM Alexa Fluor 647-dynein, 200 nM dynactin, 500 nM Egl/BicD or Egl/BicD storage buffer (GF150), and 1 µM *oskar* RNA, which was subsequently diluted 1:1 in Staufen storage buffer and processed as above.

Image analysis

Binding and motility of RNA and dynein in the in vitro reconstitution assays were manually analyzed by kymograph in FIJI (Schindelin et al. 2012) as described previously (McClintock et al. 2018). Statistical analysis and plotting were performed using GraphPad Prism version 9.1.1 for MacOS, GraphPad Software, San Diego, California USA, www.graphpad.com.

Acknowledgements

We thank the EMBL Advanced Light Microscopy and Gene Core Facilities for their support. We acknowledge Alessandra Reversi (EMBL *Drosophila* Injection Service) for fly transgenesis and thank Florence Besse for *Drosophila* strains and Dierk Niessing for reagents for recombinant Staufen expression. Work in S.L.B.'s group is supported by UK Research and Innovation (MRC file reference number MC_U105178790). M.A.M. is supported by a BBSRC project grant (BB/T00696X/1). L.-J.P. is supported by a FOR 2333 grant of the Deutsche Forschungsgemeinschaft (Germany) to A.E. A.E. gratefully acknowledges the support of the European Molecular Biology Laboratory.

Author contributions

I.G. and M.A.M. designed experiments. I.G., L.J.P., M.A.M. and S.H. carried out the experiments and analyzed the data. S.L.B. and A.E. supervised the work. All authors discussed the data and contributed to manuscript preparation.

Competing interests statement

The authors declare that there are no competing interests.

Supplementary Material

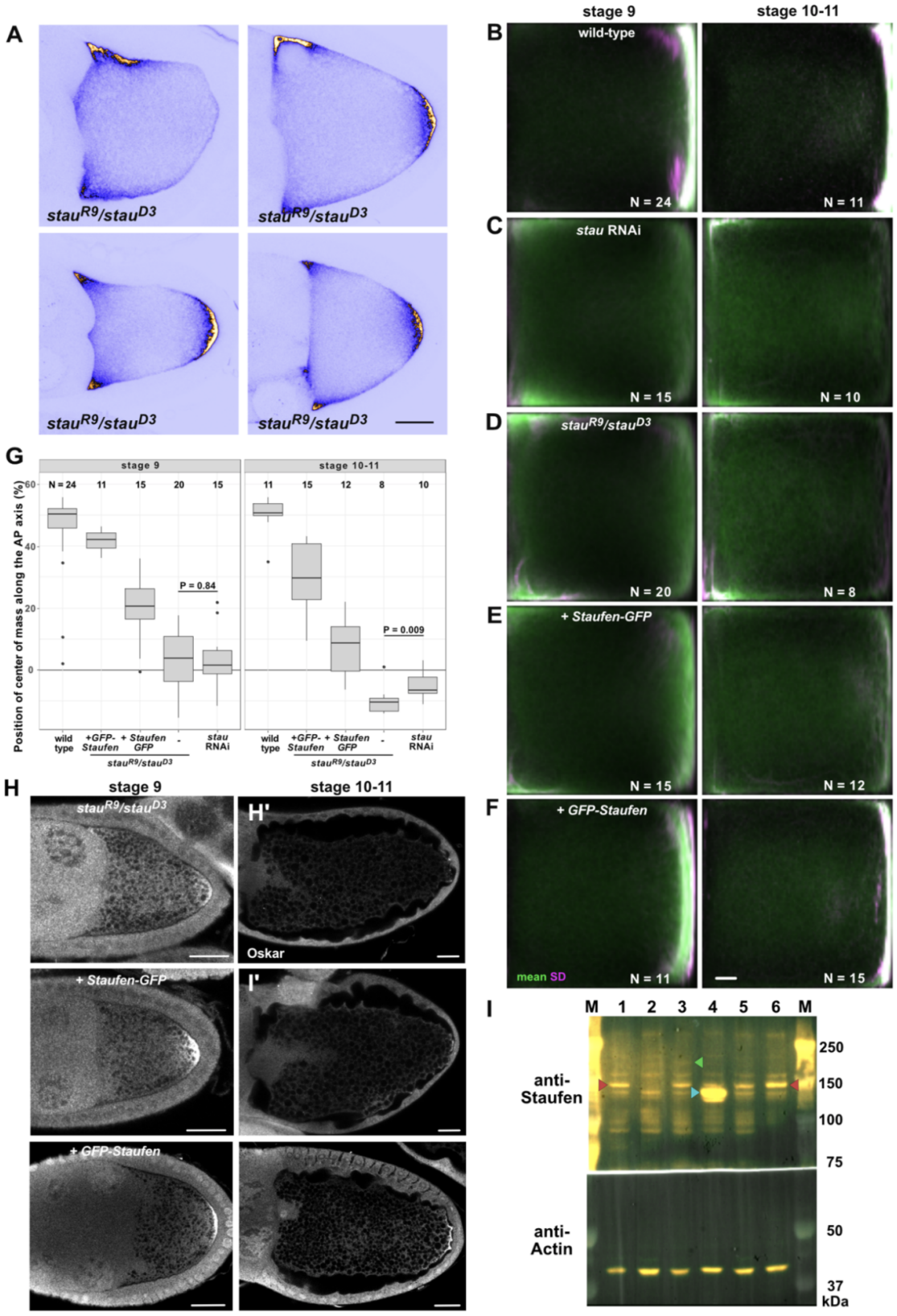

Figure S1: Expression and effect of the different Staufen transgenes on *oskar* mRNA localization.

(A) Examples of observed *oskar* RNA localization phenotypes in stage 9 *stau*^{R9}/*stau*^{D3} mutant oocytes. (B-F) Average distribution of *oskar* mRNA (green) and variability of the distribution (SD, magenta) in stage 9 and

stage 10-11 oocytes. Numbers indicate the number of oocytes analyzed for each condition, scale bar represents 10% of anteroposterior axis length. (G) Position of the *oskar* center-of-mass along the AP axis in stage 9 and stage 10-11 oocytes for each condition. 0 represents the geometric center of the oocyte, the posterior pole is located at around 58%. (H) Expression of Oskar protein in oocytes lacking Staufen, rescued by the Staufen-GFP and GFP-Staufen transgenes. (I) Western blot detection of Staufen in wild-type (lane 1), $stau^{R9}/stau^{D3}$ (2), Staufen-GFP (3), GFP-Staufen (4), *staufen* RNAi (5) and control RNAi (6) ovarian lysates. (A, H) Scale bars represent 20 microns. Note that the distribution of *oskar* in $stau^{R9}/stau^{D3}$ and in *staufen* RNAi oocytes is nearly identical (C, D and G), in spite of residual presence of Staufen in Staufen RNAi ovarian lysates (I, lanes 5 and 6). The Staufen overexpressing GFP-Staufen (I, lane 4) transgene largely rescues the *oskar* mislocalization (F and G) and Oskar protein expression defect (H) observed in the absence of Staufen. The Staufen-GFP transgene, expressed at low levels (I, lane 3), rescues *oskar* RNA localization during stage 9, but the RNA is not maintained at the posterior during stages 10-11 (E and G), most likely due to inefficient expression of Oskar protein at the posterior (H), which is essential for *oskar* mRNA anchoring at the oocyte posterior during the later stages (Vanzo and Ephrussi, 2002).

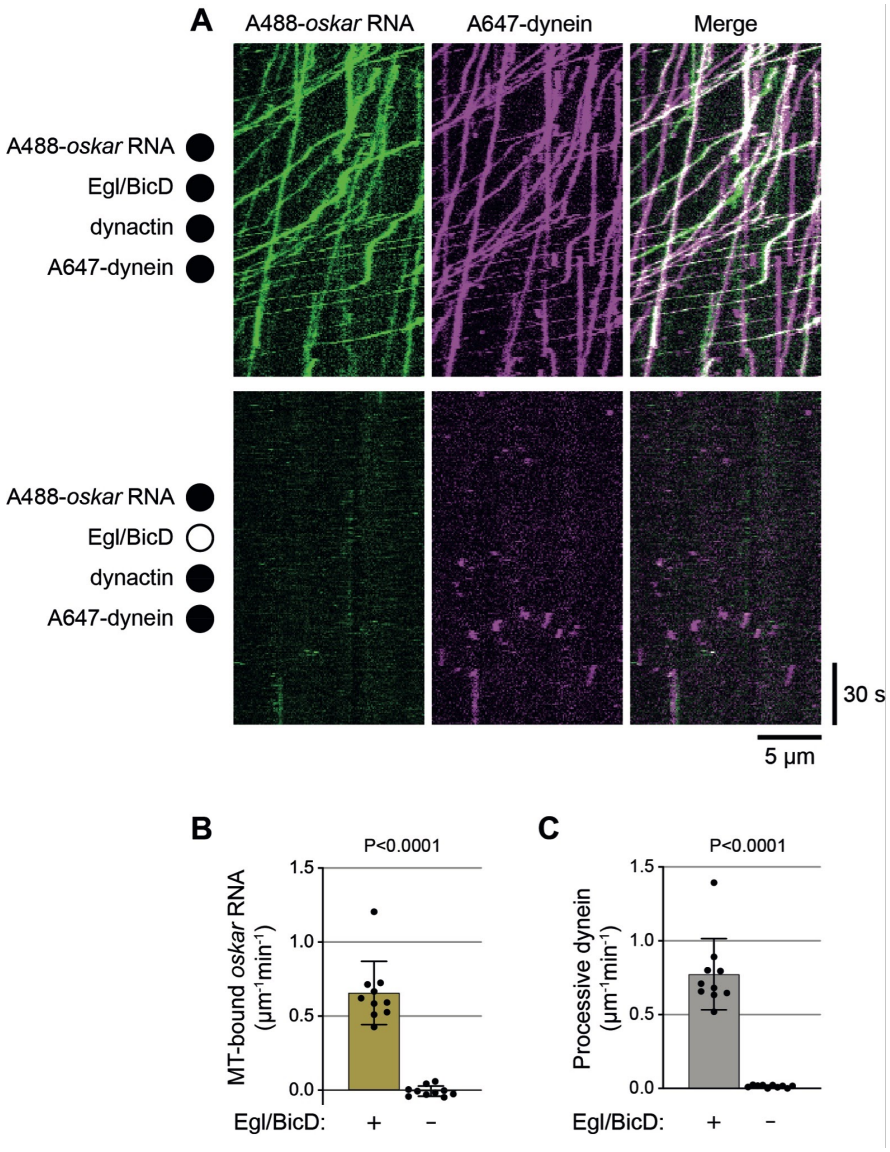

Figure S2. Egl and BicD are required for formation of transport-competent dynein-RNA complexes *in vitro*. (A) Example kymographs (time-distance plots) showing behavior of dynein and *oskar* RNA in the presence and absence of Egl and BicD; in each condition, dynactin is also present but not fluorescently labelled (filled and empty circles represent the presence and absence of indicated proteins, respectively). Egl and BicD were co-expressed and co-purified (see Methods). (B and C) Charts showing the total number of microtubule (MT) binding events for *oskar* RNA (B) and number of processive dynein complexes on microtubules under conditions shown in A. In B, values were corrected for non-specific background binding of *oskar* RNA to the imaging surface as described in Methods. Mean ± SD of values from individual microtubules (represented by black circles) are displayed. Statistical significance and P-values were determined with Mann-Whitney tests.

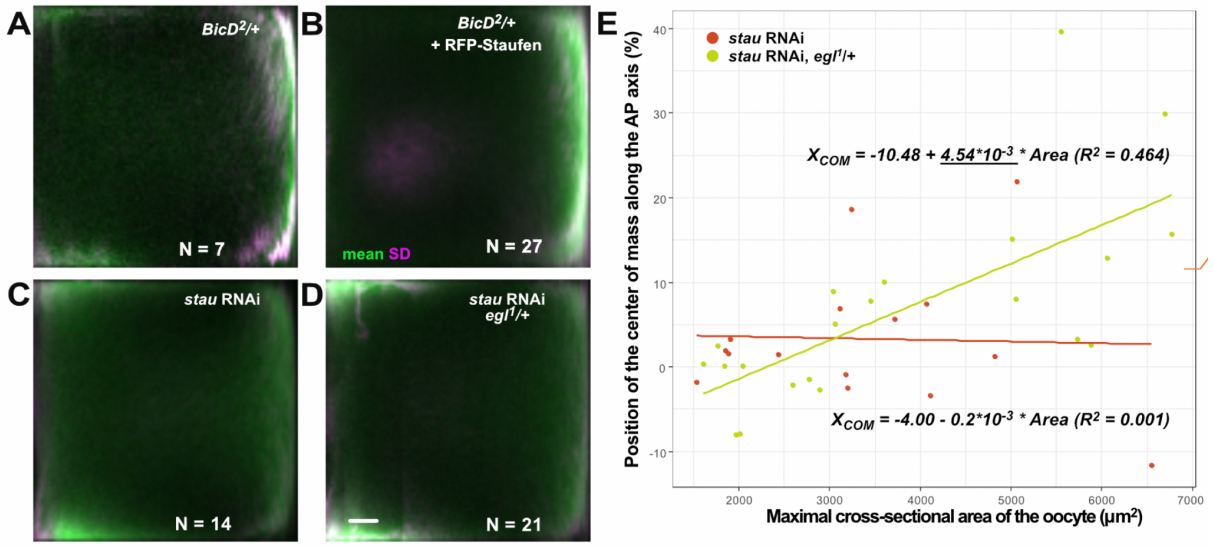

Figure S3: Suppression of *oskar* mislocalization

(A-D) Average distribution of *oskar* mRNA (green) and variability of the distribution (SD, magenta) in stage 9 oocytes of the indicated genotypes. (E) Distribution of the observed *oskar* center-of-mass in stage 9 *staufen* RNAi oocytes in the presence of two (red) or one (yellow) functional copies of e*gl*, as a function of oocyte size, which is used as a proxy for developmental time. Solid lines show the best linear fits to the data. The equation and the square of the goodness-of-fit (R^2) are indicated. Such moderate rescue was expected as *oskar* RNPs entering the oocyte are thought to be associated with the dynein cargo adapter Egl. Note that there is no significant linear correlation between oocyte size (developmental age) and the position of the center-of-mass in *stau* RNAi (red), indicating a rather static *oskar* mislocalization phenotype. There is a moderate correlation with a significant slope (underlined) when one copy of e*gl* is removed (yellow), indicating progressive posterior-ward localization of *oskar* mRNA during stage 9.

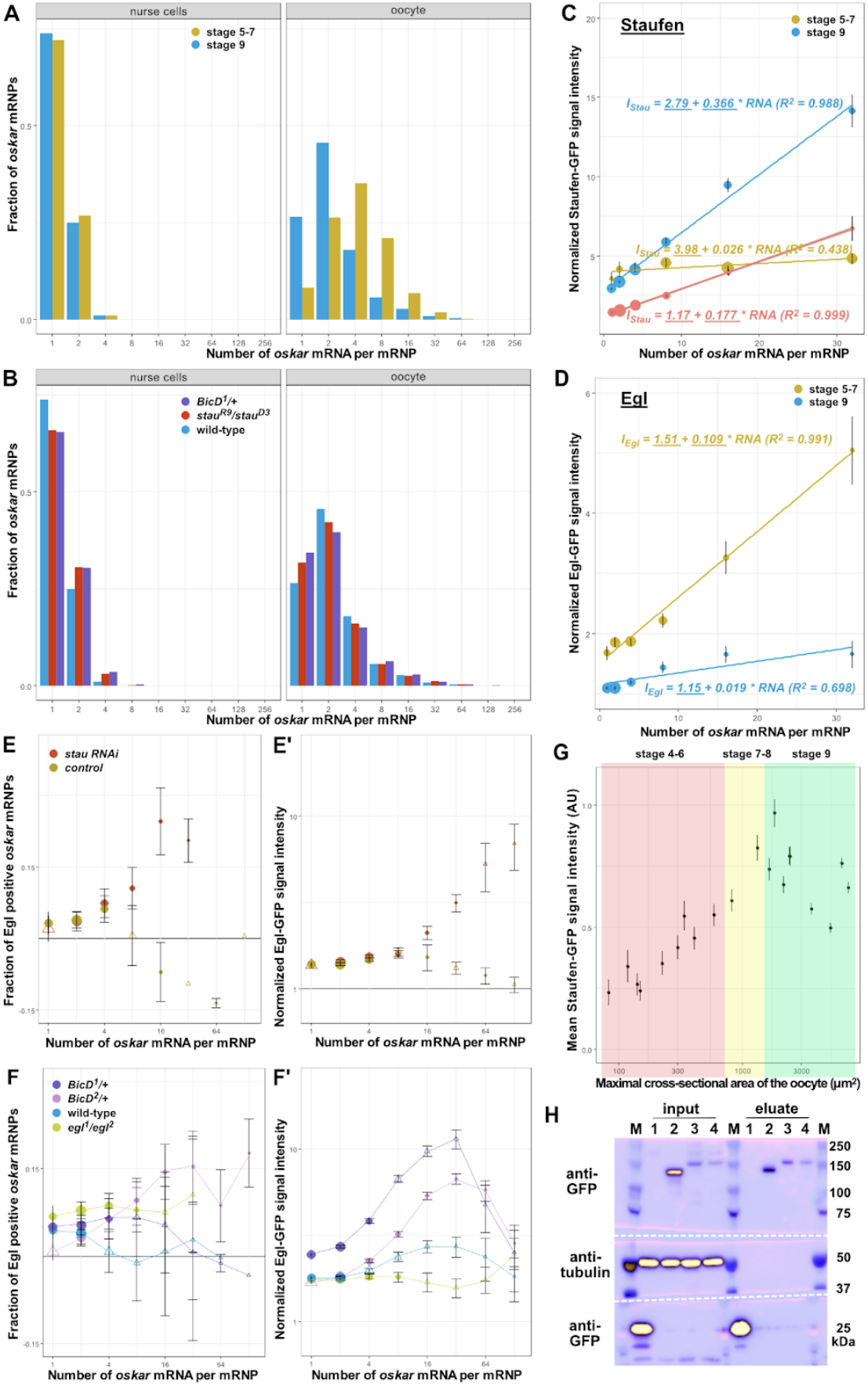
A
nurse cells
oocyte
stage 5-7
stage 9
Fraction of oskar mRNPs
Number of oskar mRNA per mRNP
B
BicD1/+
stauR9/stauD3
wild-type
C
Staufen
Normalized Staufen-GFP signal intensity
I_Stau = 2.79 + 0.366 * RNA (R² = 0.988)
I_Stau = 3.98 + 0.026 * RNA (R² = 0.438)
I_Stau = 1.17 + 0.177 * RNA (R² = 0.999)
D
Egl
Normalized Egl-GFP signal intensity
I_Egl = 1.51 + 0.109 * RNA (R² = 0.991)
I_Egl = 1.15 + 0.019 * RNA (R² = 0.698)
E
stau RNAi
control
Fraction of Egl positive oskar mRNPs
E'
Normalized Egl-GFP signal intensity
F
BicD2/+
egl1/egl2
F'
G
stage 4-6
stage 7-8
stage 9
Mean Staufen-GFP signal intensity (AU)
Maximal cross-sectional area of the oocyte (µm²)
H
input
eluate
M 1 2 3 4 M 1 2 3 4 M
anti-GFP
anti-tubulin
250
150
100
75
50
37
25
kDa

Figure S4: Association of Staufen and Egl with *oskar* mRNPs (A, B) Distribution of the RNA content of *oskar* mRNPs in nurse cells and wild-type oocytes (A) during stages 5-7 (yellow) and stage 9 (blue) of oogenesis, and (B) in the absence of Staufen (red) and in the presence of the dominant *BicD*^{1} mutant allele (purple). (A) In the nurse cells, the vast majority of *oskar* mRNPs contain 1-2 copies of the RNA, as reported previously (Little et al., 2015). RNA content of *oskar* RNPs increases in the oocytes: during stages 5-7 most appear to contain 4+ copies of the RNA; this value decreases to 2+ copies during the phase of posterior localization of *oskar* (stage 9, also see Little et al., 2015). (C, D) Normalized Staufen-GFP (B') or Egl-GFP (D', E') signal intensity as function of the mRNA content of *oskar* mRNPs during stages 5-7 (yellow) and stage 9 (blue). (C) Staufen-GFP signal intensity in the complete absence (yellow and blue) and in the presence (red) of wild-type levels of endogenous, unlabelled Staufen. (C, D) Fitted linear models of the correlation between (C) Staufen-GFP and (D) Egl-GFP signal intensity and *oskar* mRNA copy number are shown as solid lines and equations (top - stages 5-7, bottom - stage 9). Underscored parameters of the models are significantly different from zero ($p<0.05$). The slopes of the two fitted models are significantly different ($p<0.0001$, ANOVA). (E-F') Association of Egl-GFP with *oskar* mRNPs in oocytes expressing (E, E') *staufen* RNAi (red), control RNAi (brown), (F, F') *BicD*^{1} (purple) or *BicD*^{2} (pink) alleles. (E) Note that knock-down of Staufen results in an almost identical retention of Egl on *oskar* mRNPs as observed in complete absence of Staufen protein (Fig 3E, E'). (D-F') Egg-chambers expressed a single copy of Egl-GFP in the presence of two endogenous wild-type e*gl* alleles, except in the case of the rescued e*gl* mutants (F, *egl*^{1}/*egl*^{2}, green). Although in this case we observed a slightly elevated fraction of Egl positive mRNPs, larger mRNPs containing 16+ copies of *oskar* mRNA displayed no significant association with Egl (F) and the relative amounts of Egl on *oskar* mRNPs were identical to what was observed in the presence of endogenous, unlabelled Egl (F', blue). (G) Mean signal intensity of Staufen-GFP measured at multiple locations throughout developing oocytes. Size of the oocytes (x-axis) is used as a proxy of developmental time and, along with the morphological clues, for staging of the oocytes (shaded areas as indicated in the panel). (C-G) Error bars show the 95% confidence interval of the mean.(H) Western blot of input lysates and eluates after e*gl* RNA immunoprecipitation in the presence (lane 3) or the absence (lane 4) of Staufen. Bait proteins - monomeric EGFP (lane 1), GFP-Staufen (lane 2) and Egl-GFP (lanes 3,4) - are detected by anti-GFP antibody. Anti-tubulin staining served to monitor potential contamination of the eluates.

.

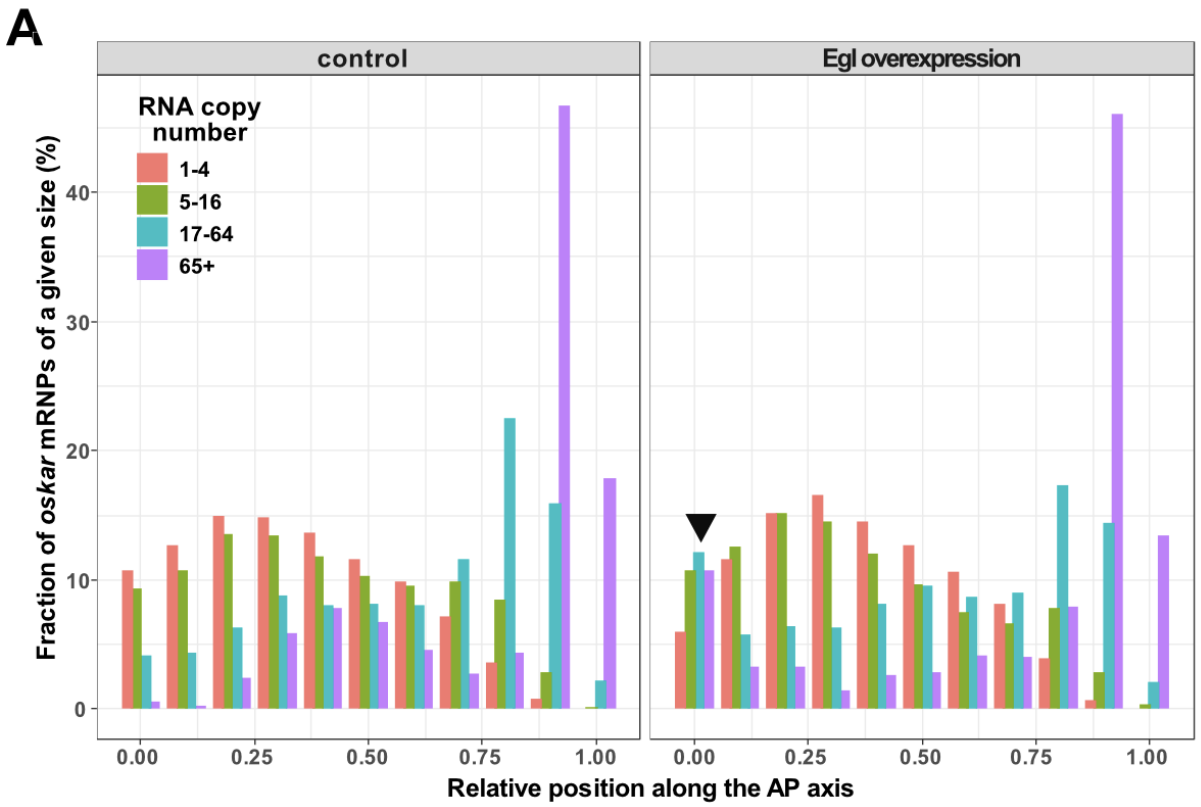

Figure S5: Localization of *oskar* mRNPs along the AP axis.
(A) Relative distribution of *oskar* mRNPs grouped by RNA content along the anteroposterior axis in wild-type and in Egl overexpressing oocytes.

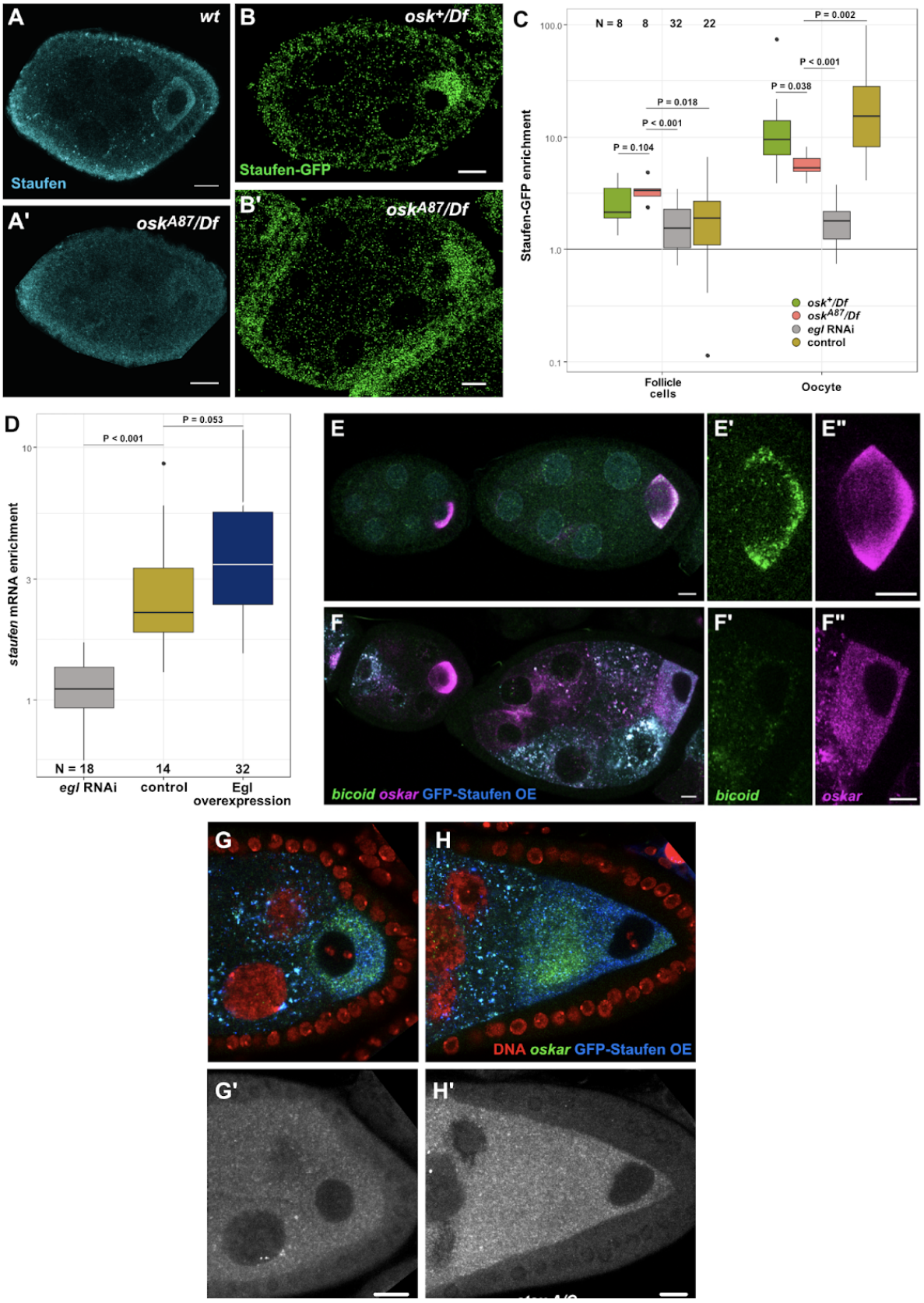
A
wt
Staufen
B
osk+/Df
Staufen-GFP
A'
oskA87/Df
B'
oskA87/Df
C
N = 8
8
32
22
P = 0.002
P < 0.001
P = 0.038
P = 0.018
P < 0.001
P = 0.104
Staufen-GFP enrichment
100.0
10.0
1.0
0.1
osk+/Df
oskA87/Df
egl RNAi
control
Follicle cells
Oocyte
D
P < 0.001
P = 0.053
staufen mRNA enrichment
10
3
1
N = 18
14
32
egl RNAi
control
Egl overexpression
E
E'
E''
F
F'
F''
bicoid oskar GFP-Staufen OE
bicoid
oskar
G
H
DNA oskar GFP-Staufen OE
G'
H'

Figure S6: Localization of Staufen protein and *staufen* mRNA in the *Drosophila* egg-chamber
(A-B') Staufen protein expression detected via immunofluorescence (blue, A and A') or by the fluorescent reporter Staufen-GFP (B and B', green) in early egg-chambers in the presence (A and B) and in complete absence of *oskar* mRNA (A' and B'). Note that lack of *oskar* from the oocyte blocks progression of oogenesis beyond stage 6 (Jenny et al., 2006). (C) Enrichment of Staufen-GFP signal in early oocytes with one (green) or no (red) functional *oskar* allele expressing *oskar* mRNA, and in oocytes expressing *egl* RNAi (grey) or control RNAi (brown). Enrichment is relative to the sibling nurse cells in the egg-chamber. Enrichment of Staufen-GFP in somatic follicle cells, which do not express the shRNA, serves as a control. P-values of pairwise Student's t-test are shown. Note that complete lack of *oskar* mRNA, an abundant binding partner of Staufen, has only a moderate effect on Staufen enrichment in the developing oocyte (also observed in A-B'), whereas knock-down of Egl almost completely abolishes Staufen ooplasmic accumulation. (D) Quantification of the enrichment of *staufen* mRNA in the oocyte – detected using the stau A/C probe set – in *egl* RNAi (grey), control RNAi (yellow) and Egalitarian overexpressing oocytes (dark blue). Note that an excess of Egl has a minuscule effect on *staufen* RNA accumulation in the oocyte, suggesting that in the wild-type, most of the *staufen* mRNA expressed in the nurse cells is transported into the oocyte. (E-F") Early egg-chambers overexpressing GFP-Staufen (F, blue) under control of the *matTub*-Gal4 driver. Note that in control oocytes of similar stage (E-E"), and in oocytes expressing low levels of GFP-Staufen (F, left egg-chamber), *oskar* mRNA (E", F", magenta) is enriched. Enrichment of *oskar* and *bicoid* (E', F', green) mRNAs is greatly reduced in oocytes expressing high levels of GFP-Staufen (F, right egg-chamber). (G-H') Early and mid-oogenetic egg-chambers overexpressing GFP-Staufen (blue) under control of the *oskar*-Gal4 driver from the beginning of oogenesis. The vast majority of such egg-chambers fail to develop beyond stage 6, (G) likely as a consequence of greatly reduced ooplasmic accumulation of *oskar* mRNA (green), which appears to be trapped in the nurse cells in large aggregates associated with GFP-Staufen. Similarly, no accumulation of *staufen* mRNA is observed in these *oskar-Gal4>UASp-GFP-Staufen* oocytes (G' and H'), where *staufen* mRNA levels are uniformly high in the germline (compare the signal in the follicle cell layer to that in the nurse cells and in the oocyte, see Figure 7). (H, H') In the oocytes occasionally escaping early developmental arrest, we invariably observed failure in nuclear migration from the posterior to the anterior, reflecting a defect in repolarization of the oocyte microtubule network (Januschke et al., 2006). Consequently, *oskar* mRNA remains in the center of these oocytes, which - although they complete oogenesis - fail to result in viable progeny. Scale bar represents 5 µm.

Video S1 and S2: Live cell imaging of *oskMS2*-GFP RNPs in control (Video S1) and *stau* RNAi (Video S2) stage 9 oocytes. Anterior (left) and posterior (right) regions of the same oocyte are shown. *oskMS2*-GFP signal is rendered in blue-yellow to allow visual appreciation of dim (blue) and bright (yellow) *oskar* mRNPs.

Video S3 and S4: Ex vivo imaging of *oskMS2*-GFP RNPs in extracts of control (Video S3) and *stau* RNAi (Video S4) stage 9 oocytes. *oskar* mRNPs are shown in green, microtubule plus tips are labeled by EB1-mCherry (magenta). Note the frequent runs of dim *oskar* mRNPs in the *stau* RNAi condition (Video S4)

References

Abouward, R., and Schiavo, G. (2021). Walking the line: mechanisms underlying directional mRNA transport and localisation in neurons and beyond. Cell. Mol. Life Sci. *78*, 2665–2681.

Akhmanova, A., and Hammer, J.A. (2010). Linking molecular motors to membrane cargo. Curr. Opin. Cell Biol. *22*, 479–487.

Amrute-Nayak, M., and Bullock, S.L. (2012). Single-molecule assays reveal that RNA localization signals regulate dynein-dynactin copy number on individual transcript cargoes. Nat. Cell Biol. *14*, 416–423.

Bauer, K.E., Segura, I., Gaspar, I., Scheuss, V., Illig, C., Ammer, G., Hutten, S., Basyuk, E., Fernández-Moya, S.M., Ehses, J., et al. (2019). Live cell imaging reveals 3'-UTR dependent mRNA sorting to synapses. Nat. Commun. *10*, 3178.

Benaglia, T., Chauveau, D., Hunter, D.R., and Young, D. (2009). mixtools : an*r* package for analyzing finite mixture models. J. Stat. Softw. *32*.

Berleth, T., Burri, M., Thoma, G., Bopp, D., Richstein, S., Frigerio, G., Noll, M., and Nüsslein-Volhard, C. (1988). The role of localization of bicoid RNA in organizing the anterior pattern of the Drosophila embryo. EMBO J. *7*, 1749–1756.

Brendza, R.P., Serbus, L.R., Duffy, J.B., and Saxton, W.M. (2000). A function for kinesin I in the posterior transport of oskar mRNA and Staufen protein. Science *289*, 2120–2122.

Clark, A., Meignin, C., and Davis, I. (2007). A Dynein-dependent shortcut rapidly delivers axis determination transcripts into the Drosophila oocyte. Development *134*, 1955–1965.

Dienstbier, M., Boehl, F., Li, X., and Bullock, S.L. (2009). Egalitarian is a selective RNA-binding protein linking mRNA localization signals to the dynein motor. Genes Dev. *23*, 1546–1558.

Eliscovich, C., and Singer, R.H. (2017). RNP transport in cell biology: the long and winding road. Curr. Opin. Cell Biol. *45*, 38–46.

Ephrussi, A., and Lehmann, R. (1992). Induction of germ cell formation by oskar. Nature *358*, 387–392.

Ephrussi, A., Dickinson, L.K., and Lehmann, R. (1991). Oskar organizes the germ plasm and directs localization of the posterior determinant nanos. Cell *66*, 37–50.

Ferrandon, D., Elphick, L., Nüsslein-Volhard, C., and St Johnston, D. (1994). Staufen protein associates with the 3'UTR of bicoid mRNA to form particles that move in a microtubule-dependent manner. Cell *79*, 1221–1232.

Gaspar, I. (2011). Microtubule-based motor-mediated mRNA localization in Drosophila oocytes and embryos. Biochem. Soc. Trans. *39*, 1197–1201.

Gaspar, I., and Ephrussi, A. (2017). Ex vivo Ooplasmic Extract from Developing Drosophila Oocytes for Quantitative TIRF Microscopy Analysis. Bio Protoc *7*.

Gaspar, I., Yu, Y.V., Cotton, S.L., Kim, D.-H., Ephrussi, A., and Welte, M.A. (2014). Klar ensures thermal robustness of oskar localization by restraining RNP motility. J. Cell Biol. *206*, 199–215.

Gaspar, I., Wippich, F., and Ephrussi, A. (2017). Enzymatic production of single-molecule FISH and RNA capture probes. RNA *23*, 1582–1591.

Gáspár, I., Sysoev, V., Komissarov, A., and Ephrussi, A. (2017). An RNA-binding atypical tropomyosin recruits kinesin-1 dynamically to oskar mRNPs. EMBO J. *36*, 319–333.

Ghosh, S., Marchand, V., Gáspár, I., and Ephrussi, A. (2012). Control of RNP motility and localization by a splicing-dependent structure in oskar mRNA. Nat. Struct. Mol. Biol. *19*, 441–449.

Glock, C., Heumüller, M., and Schuman, E.M. (2017). mRNA transport & local translation in neurons. Curr. Opin. Neurobiol. *45*, 169–177.

Gratz, S.J., Cummings, A.M., Nguyen, J.N., Hamm, D.C., Donohue, L.K., Harrison, M.M., Wildonger, J., and O'Connor-Giles, K.M. (2013). Genome engineering of Drosophila with the CRISPR RNA-guided Cas9 nuclease. Genetics *194*, 1029–1035.

Heber, S., Gáspár, I., Tants, J.-N., Günther, J., Moya, S.M.F., Janowski, R., Ephrussi, A., Sattler, M., and Niessing, D. (2019). Staufen2-mediated RNA recognition and localization requires combinatorial action of multiple domains. Nat. Commun. *10*, 1659.

Heraud-Farlow, J.E., Sharangdhar, T., Li, X., Pfeifer, P., Tauber, S., Orozco, D., Hörmann, A., Thomas, S., Bakosova, A., Farlow, A.R., et al. (2013). Staufen2 regulates neuronal target RNAs. Cell Rep. *5*, 1511–1518.

Jambor, H., Mueller, S., Bullock, S.L., and Ephrussi, A. (2014). A stem-loop structure directs oskar mRNA to microtubule minus ends. RNA *20*, 429–439.

Januschke, J., Gervais, L., Dass, S., Kaltschmidt, J.A., Lopez-Schier, H., St Johnston, D., Brand, A.H., Roth, S., and Guichet, A. (2002). Polar transport in the Drosophila oocyte requires Dynein and Kinesin I cooperation. Curr. Biol. *12*, 1971–1981.

Januschke, J., Gervais, L., Gillet, L., Keryer, G., Bornens, M., and Guichet, A. (2006). The centrosome-nucleus complex and microtubule organization in the Drosophila oocyte. Development *133*, 129–139.

Jenny, A., Hachet, O., Závorszky, P., Cyrklaff, A., Weston, M.D.J., Johnston, D.S., Erdélyi, M., and Ephrussi, A. (2006). A translation-independent role of oskar RNA in early Drosophila oogenesis. Development *133*, 2827–2833.

Kim, Y.K., Furic, L., Desgroseillers, L., and Maquat, L.E. (2005). Mammalian Staufen1 recruits Upf1 to specific mRNA 3'UTRs so as to elicit mRNA decay. Cell *120*, 195–208.

Laver, J.D., Li, X., Ancevicius, K., Westwood, J.T., Smibert, C.A., Morris, Q.D., and Lipshitz, H.D. (2013). Genome-wide analysis of Staufen-associated mRNAs identifies secondary structures that confer target specificity. Nucleic Acids Res. *41*, 9438–9460.

Lenth, R.V. (2016). Least-Squares Means: the *R* package lsmeans. J. Stat. Softw. *69*, 1–33.

Little, S.C., Sinsimer, K.S., Lee, J.J., Wieschaus, E.F., and Gavis, E.R. (2015). Independent and coordinate trafficking of single Drosophila germ plasm mRNAs. Nat. Cell Biol. *17*, 558–568.

Liu, Y., Salter, H.K., Holding, A.N., Johnson, C.M., Stephens, E., Lukavsky, P.J., Walshaw, J., and Bullock, S.L. (2013). Bicaudal-D uses a parallel, homodimeric coiled coil with heterotypic registry to coordinate recruitment of cargos to dynein. Genes Dev. *27*, 1233–1246.

Mach, J.M., and Lehmann, R. (1997). An Egalitarian-BicaudalD complex is essential for oocyte specification and axis determination in Drosophila. Genes Dev. *11*, 423–435.

Marchand, V., Gaspar, I., and Ephrussi, A. (2012). An intracellular transmission control

protocol: assembly and transport of ribonucleoprotein complexes. Curr. Opin. Cell Biol. *24*, 202–210.

Martin, K.C., and Ephrussi, A. (2009). mRNA localization: gene expression in the spatial dimension. Cell *136*, 719–730.

McClintock, M.A., Dix, C.I., Johnson, C.M., McLaughlin, S.H., Maizels, R.J., Hoang, H.T., and Bullock, S.L. (2018). RNA-directed activation of cytoplasmic dynein-1 in reconstituted transport RNPs. Elife *7*.

Micklem, D.R., Adams, J., Grünert, S., and St Johnston, D. (2000). Distinct roles of two conserved staufen domains in *oskar* mRNA localization and translation. EMBO J. *19*, 1366–1377.

Mofatteh, M., and Bullock, S.L. (2017). SnapShot: Subcellular mRNA Localization. Cell *169*, 178-178.e1.

Mohr, S., Kenny, A., Lam, S.T.Y., Morgan, M.B., Smibert, C.A., Lipshitz, H.D., and Macdonald, P.M. (2021). Opposing roles for Egalitarian and Staufen in transport, anchoring and localization of oskar mRNA in the Drosophila oocyte. PLoS Genet. *17*, e1009500.

Navarro, C., Puthalakath, H., Adams, J.M., Strasser, A., and Lehmann, R. (2004). Egalitarian binds dynein light chain to establish oocyte polarity and maintain oocyte fate. Nat. Cell Biol. *6*, 427–435.

Neuman-Silberberg, F.S., and Schüpbach, T. (1993). The drosophila dorsoventral patterning gene gurken produces a dorsally localized RNA and encodes a TGFα-like protein. Cell *75*, 165–174.

Palacios, I.M., and St Johnston, D. (2002). Kinesin light chain-independent function of the Kinesin heavy chain in cytoplasmic streaming and posterior localisation in the Drosophila oocyte. Development *129*, 5473–5485.

Park, E., Gleghorn, M.L., and Maquat, L.E. (2013). Staufen2 functions in Staufen1-mediated mRNA decay by binding to itself and its paralog and promoting UPF1 helicase but not ATPase activity. Proc Natl Acad Sci USA *110*, 405–412.

Parton, R.M., Hamilton, R.S., Ball, G., Yang, L., Cullen, C.F., Lu, W., Ohkura, H., and Davis, I. (2011). A PAR-1-dependent orientation gradient of dynamic microtubules directs posterior cargo transport in the Drosophila oocyte. J. Cell Biol. *194*, 121–135.

Rom, I., Faicevici, A., Almog, O., and Neuman-Silberberg, F.S. (2007). Drosophila Dynein light chain (DDLC1) binds to gurken mRNA and is required for its localization. Biochim. Biophys. Acta *1773*, 1526–1533.

R Core Team (2014). R: A language and environment for statistical computing. R Foundation for StatisticalComputing.

Sanghavi, P., Laxani, S., Li, X., Bullock, S.L., and Gonsalvez, G.B. (2013). Dynein associates with oskar mRNPs and is required for their efficient net plus-end localization in Drosophila oocytes. PLoS ONE *8*, e80605.

Sanghavi, P., Liu, G., Veeranan-Karmegam, R., Navarro, C., and Gonsalvez, G.B. (2016). Multiple roles for egalitarian in polarization of the drosophila egg-chamber. Genetics *203*, 415–432.

Schuldt, A.J., Adams, J.H., Davidson, C.M., Micklem, D.R., Haseloff, J., St Johnston, D., and

Brand, A.H. (1998). Miranda mediates asymmetric protein and RNA localization in the developing nervous system. Genes Dev. *12*, 1847–1857.

Schüpbach, T., and Wieschaus, E. (1989). Female sterile mutations on the second chromosome of Drosophila melanogaster. I. Maternal effect mutations. Genetics *121*, 101–117.

Sladewski, T.E., Billington, N., Ali, M.Y., Bookwalter, C.S., Lu, H., Krementsova, E.B., Schroer, T.A., and Trybus, K.M. (2018). Recruitment of two dyneins to an mRNA-dependent Bicaudal D transport complex. Elife *7*.

St Johnston, D. (2005). Moving messages: the intracellular localization of mRNAs. Nat. Rev. Mol. Cell Biol. *6*, 363–375.

St Johnston, D., Beuchle, D., and Nüsslein-Volhard, C. (1991). Staufen, a gene required to localize maternal RNAs in the Drosophila egg. Cell *66*, 51–63.

St Johnston, D., Brown, N.H., Gall, J.G., and Jantsch, M. (1992). A conserved double-stranded RNA-binding domain. Proc Natl Acad Sci USA *89*, 10979–10983.

Sysoev, V.O., Fischer, B., Frese, C.K., Gupta, I., Krijgsveld, J., Hentze, M.W., Castello, A., and Ephrussi, A. (2016). Global changes of the RNA-bound proteome during the maternal-to-zygotic transition in Drosophila. Nat. Commun. *7*, 12128.

Trovisco, V., Belaya, K., Nashchekin, D., Irion, U., Sirinakis, G., Butler, R., Lee, J.J., Gavis, E.R., and St Johnston, D. (2016). bicoid mRNA localises to the Drosophila oocyte anterior by random Dynein-mediated transport and anchoring. Elife *5*.

Vanzo, N.F., and Ephrussi, A. (2002). Oskar anchoring restricts pole plasm formation to the posterior of the Drosophila oocyte. Development *129*, 3705–3714.

Vazquez-Pianzola, P., Schaller, B., Colombo, M., Beuchle, D., Neuenschwander, S., Marcil, A., Bruggmann, R., and Suter, B. (2017). The mRNA transportome of the BicD/Egl transport machinery. RNA Biol. *14*, 73–89.

Wickham, H. (2016). ggplot2 - Elegant Graphics for Data Analysis (New York, NY: Springer-Verlag New York).

Williams, L.S., Ganguly, S., Loiseau, P., Ng, B.F., and Palacios, I.M. (2014). The auto-inhibitory domain and ATP-independent microtubule-binding region of Kinesin heavy chain are major functional domains for transport in the Drosophila germline. Development *141*, 176–186.

Wu, B., Chao, J.A., and Singer, R.H. (2012). Fluorescence fluctuation spectroscopy enables quantitative imaging of single mRNAs in living cells. Biophys. J. *102*, 2936–2944.

Zimyanin, V.L., Belaya, K., Pecreaux, J., Gilchrist, M.J., Clark, A., Davis, I., and St Johnston, D. (2008). In vivo imaging of oskar mRNA transport reveals the mechanism of posterior localization. Cell *134*, 843–853.